Human myocytes are protected from titin aggregation-induced stiffening by small heat shock proteins

Sebastian Kötter,[1] Andreas Unger,[1] Nazha Hamdani,[1] Patrick Lang,[1] Matthias Vorgerd,[2] Luitgard Nagel-Steger,[3] and Wolfgang A. Linke[1]

[1]Department of Cardiovascular Physiology and [2]Neurological University Clinic Bergmannsheil, Ruhr University Bochum, 44780 Bochum, Germany
[3]Department of Physical Biology, University of Düsseldorf, 40225 Düsseldorf, Germany

In myocytes, small heat shock proteins (sHSPs) are preferentially translocated under stress to the sarcomeres. The functional implications of this translocation are poorly understood. We show here that HSP27 and αB-crystallin associated with immunoglobulin-like (Ig) domain-containing regions, but not the disordered PEVK domain (titin region rich in proline, glutamate, valine, and lysine), of the titin springs. In sarcomeres, sHSP binding to titin was actin filament independent and promoted by factors that increased titin Ig unfolding, including sarcomere stretch and the expression of stiff titin isoforms. Titin spring elements behaved predominantly as monomers in vitro. However, unfolded Ig segments aggregated, preferentially under acidic conditions, and αB-crystallin prevented this aggregation. Disordered regions did not aggregate. Promoting titin Ig unfolding in cardiomyocytes caused elevated stiffness under acidic stress, but HSP27 or αB-crystallin suppressed this stiffening. In diseased human muscle and heart, both sHSPs associated with the titin springs, in contrast to the cytosolic/Z-disk localization seen in healthy muscle/heart. We conclude that aggregation of unfolded titin Ig domains stiffens myocytes and that sHSPs translocate to these domains to prevent this aggregation.

Introduction

HSP27 (HSPB1) and αB-crystallin (HSPB5) are members of the family of small heat shock proteins (sHSPs) ubiquitously expressed in mammalian tissues (Klemenz et al., 1993). sHSPs are important components of the cellular protein quality control machinery as they bind partially unfolded client proteins, hold them in a folding-prone state, and protect them from aggregation (Mymrikov et al., 2011). They are also directly linked to the autophagy and proteasomal degradation pathways (Willis and Patterson, 2010). Typically, sHSPs are up-regulated under diverse stress situations, and their overexpression protects cells from oxidative stress, energy depletion, and other unfavorable conditions (Mymrikov et al., 2011). In the heart, αB-crystallin and HSP27 are induced during ischemic injury, heat stress, or end-stage failure (Martin et al., 1997; Benjamin and McMillan, 1998; Knowlton et al., 1998; Yoshida et al., 1999; Dohke et al., 2006; Li et al., 2012). Induction of sHSPs also occurs in both myopathic skeletal (Kley et al., 2012) and normal muscles after intense exercise (Paulsen et al., 2009) and during aging (Doran et al., 2007).

In response to potentially harmful insults, the myocyte sHSPs, including αB-crystallin and HSP27, preferentially translocate from the cytosol to the myofibrils, where they bind to the sarcomeric Z-disk and/or I-band (Barbato et al., 1996; Lutsch et al., 1997; van de Klundert et al., 1998; Golenhofen et al., 1999; Fischer et al., 2002; Paulsen et al., 2009). Whether or not this translocation depends on the phosphorylation state of sHSPs is controversial (Mymrikov et al., 2011). Sarcomere proteins suggested to be protected by sHSP binding include desmin, α-actinin, actin, troponin-I/-T, titin, and myosin (Bennardini et al., 1992; Liu and Steinacker, 2001; Golenhofen et al., 2002; Wang et al., 2003; Bullard et al., 2004; Golenhofen et al., 2004;

Correspondence to Wolfgang A. Linke: wolfgang.linke@rub.de

S. Kötter's present address is Department of Cardiovascular Physiology, University of Düsseldorf, 40225 Düsseldorf, Germany.

Abbreviations used in this paper: DCM, dilated cardiomyopathy; Ig, immunoglobulin-like; LGMD2A, limb girdle muscular dystrophy type 2A; sHSPs, small heat shock proteins; SL, sarcomere length.

© 2014 Kötter et al. This article is distributed under the terms of an Attribution–Noncommercial–Share Alike–No Mirror Sites license for the first six months after the publication date (see http://www.rupress.org/terms). After six months it is available under a Creative Commons License (Attribution–Noncommercial–Share Alike 3.0 Unported license, as described at http://creativecommons.org/licenses/by-nc-sa/3.0/).

The Rockefeller University Press $30.00
J. Cell Biol. Vol. 204 No. 2 187–202
www.jcb.org/cgi/doi/10.1083/jcb.201306077

Melkani et al., 2006; Singh et al., 2007; Lu et al., 2008; Morton et al., 2009; Paulsen et al., 2009). The protective effect of αB-crystallin on desmin is well supported by genetic evidence (Vicart et al., 1998; Wang et al., 2003). However, in stressed myocytes, HSP27 and αB-crystallin can localize to the I-band region outside the Z-disk (Lutsch et al., 1997; Golenhofen et al., 1999, 2002, 2004; Bullard et al., 2004) where desmin and α-actinin are not present. Even though the two sHSPs interact with actin stress fibers, including cytoskeletal actin fibers in premature cardiomyocytes (Verschuure et al., 2002; Singh et al., 2007), it is not clear whether they associate with sarcomeric actin. Furthermore, the protective effect of sHSPs on isolated muscle myosin (Melkani et al., 2006; Markov et al., 2008) is difficult to reconcile with Z-disk–I-band (but not A-band) localization. The I-band association may be best explained by sHSP binding to titin spring elements (Golenhofen et al., 2002; Bullard et al., 2004), which has been confirmed for mammalian αB-crystallin (Bullard et al., 2004) and tentatively proposed for zebrafish HSP27 (Tucker and Shelden, 2009).

The observation that sHSPs are induced during ischemia suggests that acidic stress is a potential trigger. Acidosis resulting from ischemia-reperfusion injury (along with oxidative stress) can be substantial in the heart, with reductions in intracellular pH by 0.5–1 units (Vaughan-Jones et al., 2009). In skeletal muscle, metabolic acidosis during physical exercise was correlated with a reduction in the intracellular pH by 0.3–0.4 units (Khong et al., 2001). Acidic conditions directly affect sHSPs by promoting the formation and accumulation of large oligomers, thereby increasing chaperone activity (Ehrnsperger et al., 1999; Chernik et al., 2004). Acidosis also promotes the aggregation of many sHSP client proteins, such as actin and desmin, whereas the sHSPs themselves provide increased protection from aggregation at reduced pH (Bennardini et al., 1992; Barbato et al., 1996). Contractility of myocytes is strongly affected by intracellular acidosis (Orchard and Kentish, 1990). Studies also suggested that acidosis increases the passive stiffness of the heart (Berger et al., 1999) and of skeletal muscles (Miyake et al., 2003). Intracellular acidosis induced by ischemic stress caused severe diastolic dysfunction in a double-knockout mouse model deficient for αB-crystallin and HSPB2 (Golenhofen et al., 2006; Pinz et al., 2008). These findings suggest a relationship among acidosis, sHSP induction, and muscle elasticity.

The elasticity and passive stiffness of striated muscle cells are influenced by titin (Linke and Krüger, 2010), an essential component of the sarcomere (da Silva Lopes et al., 2011) and the largest known protein with a molecular mass of 3,000–3,800 kD, depending on the isoform (Bang et al., 2001). The titin isoforms differ primarily in their elastic I-band region (Fig. 1 A), which can be short and relatively stiff (cardiac N2B) or longer and more compliant (cardiac N2BA and skeletal muscle N2A). These titin springs are composed of tandem repeats of folded immunoglobulin-like (Ig) domains grouped into proximal, middle, and distal (to the Z-disk) segments, an N2-A region containing four Ig domains, and two large intrinsically disordered regions: the PEVK domain (titin region rich in proline, glutamate, valine, and lysine) and the N2-B-unique sequence (N2-Bus), which is found exclusively in cardiac titin. The N2-Bus and certain Ig domains were shown previously to interact with αB-crystallin (Bullard et al., 2004), which exerted a stabilizing effect on these domains in vitro (Bullard et al., 2004; Zhu et al., 2009). However, sarcomere stretch unfolds titin domains (Rief et al., 1997; Minajeva et al., 2001), exposing concealed hydrophobic sites, which can lead to aggregation and loss of function. We hypothesized that binding of HSP27/αB-crystallin to unfolded titin domains prevents titin aggregation under stress, thereby maintaining normal myocyte stiffness. We showed that the two sHSPs specifically protect the unfolded Ig regions of titin, but not the intrinsically disordered segments (N2-Bus and PEVK), from aggregating under acidic stress. HSP27 and αB-crystallin were found to translocate preferentially to the titin springs in stretched sarcomeres as well as in diseased human skeletal and cardiac myocytes. This suggests that sHSPs indeed act to prevent abnormally high, titin aggregation-induced, passive tension. This protective mechanism for titin may apply to other "mechanical" proteins in a variety of cell types.

Results

Titin spring elements act as monomers in vitro

To obtain information about the molecular organization of titin spring elements, we performed sedimentation-velocity experiments for recombinant human N2-Bus and PEVK (both intrinsically disordered structures), the N2-B region (N2-Bus plus three Ig domains), and the N2-A segment (four Ig domains). For all constructs, the tests showed a dominant single peak in the continuous sedimentation distribution c(s) with $s_{20,w}$ values of 2.74 S (N2-Bus), 3.19 S (N2-B), 3.27 S (N2-A), and 1.06 S (PEVK; Fig. 1, B–E). Sedimentation depends, in part, on the size and shape of the molecule and is inversely proportional to the frictional ratio (f/f_0), the latter of which was 2.2 (N2-Bus and N2-B), 1.4 (N2-A), and 2.3 (PEVK). N2-Bus, N2-B, and PEVK were predicted to exist in a slightly extended conformation and N2-A in a more globular-like structure. For each titin construct, the $s_{20,w}$ value of the dominant peak corresponded to the monomeric form of the respective fragment. A minor $s_{20,w}$ value peak, suggestive of a small subpopulation of dimers (∼5–15%), was apparent for N2-Bus (4.18 S), N2-B (4.77 S), and N2-A (5.13 S; Fig. 1, B–E). Higher oligomeric states were not detected. The additional, relatively low *s* value peaks seen for N2-B and PEVK (Fig. 1, D and E) likely resulted from degradation products or contaminants. Thus, the titin spring elements behaved in vitro primarily as monomers.

In addition, size-exclusion chromatography was performed to independently test the molecular organization of two representative human titin spring regions: the four-Ig construct I9-12 (proximal Ig region) and PEVK. I9-12 was predicted to be monomeric and PEVK to be monomeric or dimeric, with no distinction possible because of the low mass of PEVK relative to the peak width (Fig. 1, F and G). These findings are consistent with the results of the sedimentation-velocity tests, suggesting that the elastic titin segment between the Z-disk–I-band junction and the distal Ig region exists primarily in a monomeric state.

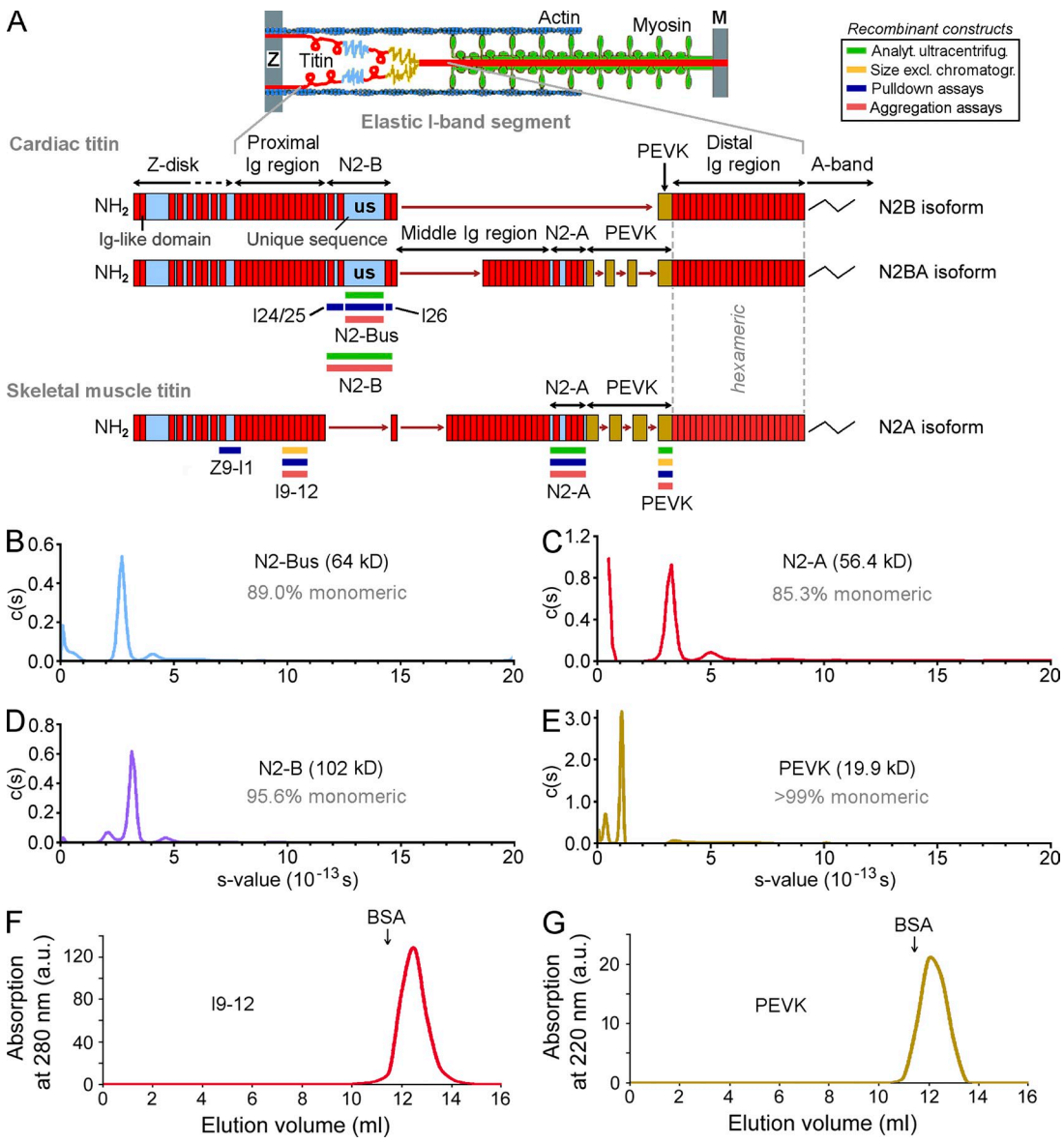

Figure 1. **The arrangement of I-band titin in the sarcomere and the existence of titin spring elements in a monomeric state.** (A) Schematic of a half sarcomere and the I-band domains of the three main human titin isoforms. The recombinant titin constructs generated for the various in vitro assays of this study are shown. (B–E) Continuous sedimentation-coefficient distributions, c(s), calculated from sedimentation-velocity experiments for purified recombinant titin constructs in medium ionic-strength buffer at 20°C. (B) Titin N2-Bus (13 µmol/l) at 52,000 rpm; (C) N2-B (5 µmol/l) at 45,000 rpm; (D) N2-A (9.5 µmol/l) at 47,000 rpm; and (E) PEVK (63 µmol/l) at 50,000 rpm. Absorbances were measured at 280 nm (220 nm for PEVK) and analyzed using SedFit. (F and G) The behavior of two representative I-band titin segments in size-exclusion chromatography experiments performed at room temperature. (F) The four-Ig domain fragment I9-12 (41.3 kD) and (G) PEVK (19.9 kD). Note that the peak heights are not comparable because of the different protein concentrations used. BSA (66 kD) was used as the elution marker.

HSP27 and αB-crystallin bind to distinct I-band titin domains

To determine which titin spring elements interact with HSP27 and αB-crystallin, we used recombinant human sHSPs and titin constructs in GST pulldown assays (Fig. 2). The two sHSPs associated with the Ig domains I24/25 (part of N2-B), the intrinsically disordered N2-Bus, and the Ig-rich N2-A region, but not with the Z9-I1 construct from the Z-disk–I-band junction (Fig. 2, A and B). Independent binding assays using the yeast two-hybrid system confirmed the interaction between N2-Bus and HSP27 or αB-crystallin (Fig. S1 A). Additional GST pulldown assays demonstrated HSP27 binding to Ig domains I9-12 and I26 (part of N2-B), but not to PEVK (Fig. 2 A). We speculated that the phosphorylation state of HSP27 may be important for the interaction with titin domains, and thus we generated phosphomimicking mutants of human HSP27 to test their binding to N2-Bus in GST pulldown assays. However, relative to the affinity of N2-Bus for wild-type HSP27, none of the mutant HSP27 constructs (single point mutants: S15D and S82D; double mutant: S15/82D; and triple mutant: S15/78/82D) showed significantly altered binding affinity (Fig. S1 B). Therefore, the binding sites for HSP27 on the elastic titin segment were similar to those for αB-crystallin and included Ig-rich segments and the N2-B region, but not PEVK (Fig. 2 C). Interaction

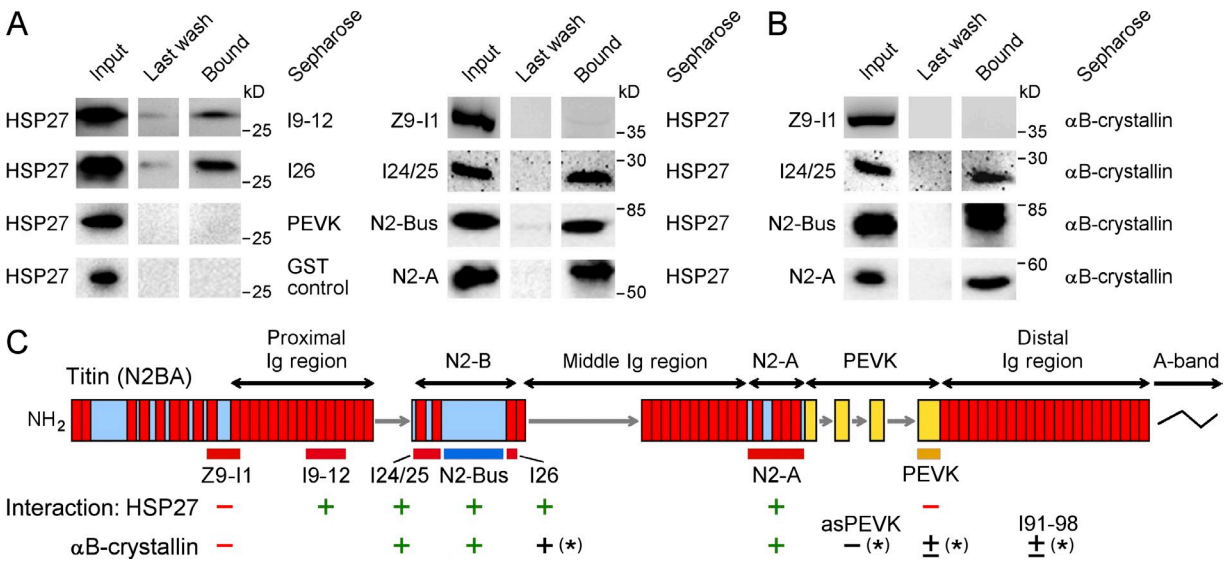

Figure 2. **The interaction between I-band titin domains and sHSPs in GST pulldown assays.** Representative Western blots demonstrating the presence or absence of an interaction of HSP27 (A) or αB-crystallin (B) with various I-band titin domains. (C) Overview of HSP27 and αB-crystallin interaction sites on I-band titin detected by this assay. Results marked by as asterisk were obtained previously (Bullard et al., 2004). The I9-12 Ig segment likely also binds αB-crystallin (Zhu et al., 2009). asPEVK, alternatively spliced PEVK.

between HSP27 and N2-Bus is unlikely to be regulated by HSP27 phosphorylation.

sHSPs bind to the sarcomeric I-band region in isolated myofibrils

To determine the region of the sarcomere that sHSPs bind, we attached the ends of human cardiomyofibrils coexpressing the N2B (∼65%) and N2BA (∼35%) titin isoforms or the ends of rabbit psoas myofibrils expressing the N2A isoform to glass needle tips to stretch the preparations (Fig. 3 A). Endogenous HSP27 and αB-crystallin were nearly absent from these isolated myofibrils. The myofibrils were incubated with excess amounts of recombinant HSP27 (Fig. 3, B and E) or αB-crystallin (Fig. 3, C and F), the unbound sHSPs were washed away, and myofibril-bound sHSPs were visualized by indirect immunofluorescence. In the control experiments, incubation with GFP or with secondary antibodies alone did not produce any specific immunofluorescence signal (Fig. 3 A). In human cardiomyofibrils, exogenous HSP27 and αB-crystallin both marked the Z-disk–I-band region when the sarcomere length (SL) was 2.4 µm but were clearly observed in the region of the I-band when the SL was 3.0 µm, as indicated by the appearance of double bands (Fig. 3, B and C). Importantly, even after gelsolin-mediated extraction of actin filaments and associated regulatory proteins from the cardiomyofibrils, exogenous HSP27 still localized to the I-bands; the Z-disk (which still contained some nonextractable actin) again did not appear to be the predominant binding site (Fig. 3 D). In stretched rabbit psoas myofibrils (3.4 µm SL), I-band localization of the sHSPs was apparent, although the doublets appeared fuzzier than in the cardiomyofibrils (Fig. 3, E and F). Importantly, when the SL was 2.2 µm, HSP27 did not bind to skeletal myofibrils (Fig. 3 E) and αB-crystallin showed decreased binding to the Z-disk–I-band (Fig. 3 F). Faint staining of the sarcomeric M-band was sometimes observed (Fig. 3 E), but the sHSPs were absent from the remainder of the A-band. These results show that HSP27 and αB-crystallin bound to the extensible segment outside the Z-disk where the titin springs are located, independently of the presence of actin filaments. sHSP binding to the I-band was greatly promoted by sarcomere stretch especially in skeletal myofibrils expressing the N2A isoform lacking the N2-B domain.

Aggregation of partially denatured titin Ig domains and protection by sHSPs

We first used the TANGO algorithm (Linding et al., 2004) to predict the aggregation propensity of unfolded Ig-rich and disordered I-band titin segments. The tendency for β aggregation was highest for Ig domains I9-12 (up to nearly 100%), followed by the N2-A segment (>60%) and the N2-Bus (<50%), whereas PEVK was predicted to have no aggregation propensity at all (Fig. S2). Z9-I1 from the Z-disk–I-band junction (which like PEVK did not bind sHSPs; Fig. 2) also appeared unlikely to aggregate. The α-aggregation propensity was small for all segments.

To experimentally test these predictions, recombinant titin constructs were exposed to urea, followed by rapid dilution in pH 7.2 Tris/HCl buffer, to promote their partial denaturation and potential aggregation. These conditions failed to induce aggregation of the mostly disordered titin segments N2-Bus, N2-B, and PEVK (Fig. 4 A). In contrast, I9-12 did aggregate, as indicated by increased light scattering (the absorbance at 320 nm), which plateaued at ∼20 min, whereas N2-A did not aggregate at normal pH (Fig. 4 B). However, when the pH was lowered to 6.7, N2-A aggregated more than did I9-12 (Fig. 4 B). The disordered titin segments still showed no significant aggregation at pH 6.7 (Fig. 4 A). These results were largely consistent with the TANGO predictions.

We then used this assay to test whether aggregation of denatured N2-A can be prevented by sHSPs. The presence of αB-crystallin reduced the aggregation of N2-A partially at an

N2A/αB-crystallin molar ratio of 1:5 (~75% reduction relative to the control at 30 min) and almost completely at a molar ratio of 1:10 (96% reduction; Fig. 4 C). HSP27 did not prevent aggregation of N2-A under these conditions (Fig. 4 D).

sHSPs protect overstretched cardiomyocytes from stiffening under acidic stress

Aggregation of unfolded Ig domains of the elastic titin region may affect the passive stiffness of myocytes. We measured the passive force ($F_{passive}$) of isolated skinned human cardiomyocytes in response to stepwise stretching, first in relaxing buffer at a normal pH of 7.4 and then after a 10-min prestretch to a SL of 2.6 µm (to increase the probability of titin Ig domain unfolding) in acidic pH 6.6 relaxing buffer, in the absence or presence of recombinant human sHSPs (Fig. 5 A).

The $F_{passive}$-SL curve was steeper under the acidic, prestretch conditions than under control conditions (Fig. 5, C and E). However, the increase in $F_{passive}$ failed to occur in the presence of HSP27 (Fig. 5 C) or αB-crystallin (Fig. 5 E). The protective effect on the $F_{passive}$ (at 2.2 µm SL) was similar among HSP27 concentrations of 0.01, 0.1, and 1 mg/ml (Fig. 5 C, inset), whereas greater effects were observed with higher compared with lower αB-crystallin concentrations (Fig. 5 E, inset). If the prestretch step was omitted, the $F_{passive}$-SL curve was not significantly altered by low pH alone (Fig. 5 B). Likewise, in single isolated cardiac or skeletal myofibrils, the dynamic passive stiffness, measured as the force response to 20-Hz small oscillatory length changes, was independent of pH in the 5.9–7.4 range (Fig. S3). Prestretching of human cardiomyocytes in normal pH buffer again did not alter the $F_{passive}$-SL curve (Fig. 5, D and F), and under these conditions, the presence of HSP27 (Fig. 5 D) or αB-crystallin (Fig. 5 F) had no significant effect on the $F_{passive}$. Notably, the prevention of an increase in the $F_{passive}$ by sHSPs under acidic conditions is contrary to what we initially expected according to single-molecule mechanical measurements of recombinant titin constructs (Bullard et al., 2004; Zhu et al., 2009), the results of which suggested that the titin-based force increases in the presence of sHSPs (Fig. S4 A). Instead, the sHSPs protected myocytes from becoming stiffer under acidic stress when titin Ig domains increasingly unfolded, i.e., under conditions that promote Ig aggregation.

sHSPs localize at the I-bands in myocytes with stiff titin but not in those with compliant titin

If unfolding of Ig domains is critical for titin aggregation and protection by sHSP, then sHSP binding to titin would be unlikely to occur in myocytes expressing extremely compliant titin because the Ig domains would have a very low probability of unfolding, even in stretched sarcomeres. Fetal (day 18) rat cardiomyocytes express a highly compliant (~3.7 MDa) N2BA titin isoform (Opitz et al., 2004), which the entropic elasticity theory predicts to lack Ig unfolding (Li et al., 2002) within and even beyond the physiological SL range (Fig. 6 A and Fig. S4 B) In contrast, adult rat cardiomyocytes almost exclusively express

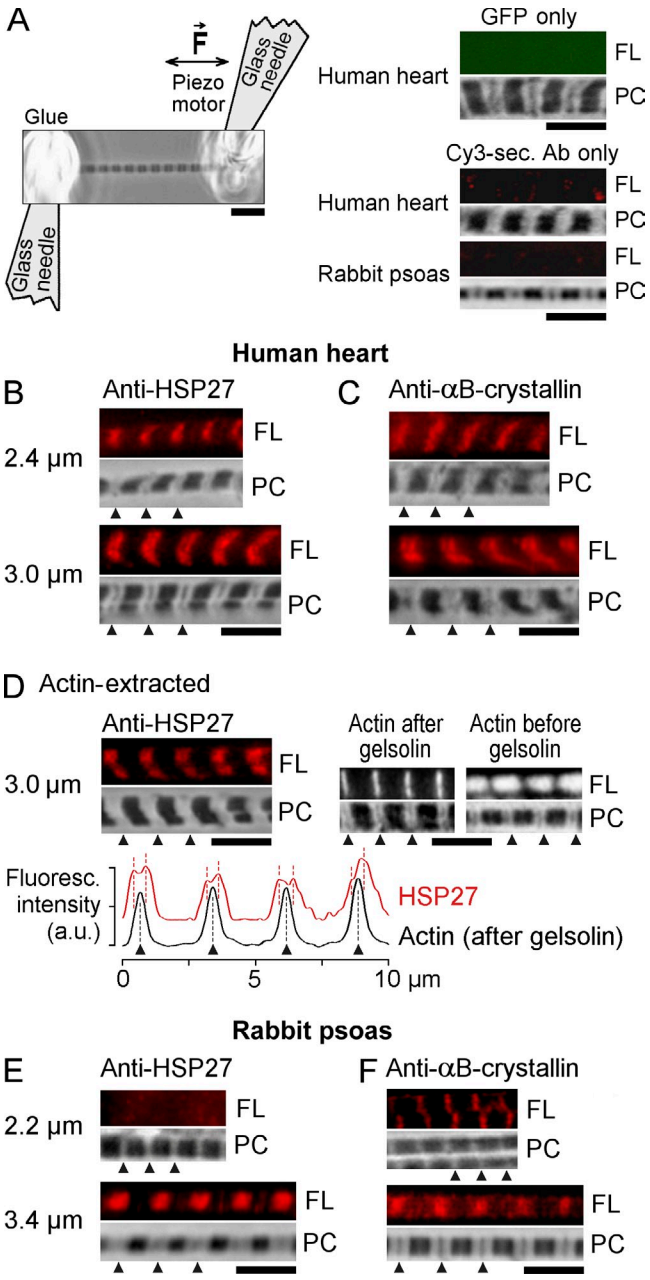

Figure 3. **Binding of exogenous HSP27 and αB-crystallin to the I-band region of isolated myofibrils.** (A) The experimental design for the stretching of single myofibrils as well as images of stretched myofibrils incubated in relaxing buffer with GFP or with Cy3-conjugated secondary antibodies alone (negative controls). Representative immunofluorescence (FL) and phase-contrast (PC) images of human cardiac (B–D) and rabbit psoas myofibrils (E and F) incubated with recombinant sHSP at the SL indicated on left. Binding was visualized using anti-sHSP primary and Cy3-conjugated secondary antibodies. (B, D, and E) Exogenous HSP27 visualized by anti-HSP27 staining. (C and F) Exogenous αB-crystallin visualized by anti-αB-crystallin staining. In D, the actin filaments were extracted from human cardiac myofibrils using a Ca^{2+}-independent gelsolin fragment before incubation with HSP27 and antibodies; images on the right demonstrate the efficient removal of actin, except in a narrow portion of the Z-disk. The profile plot taken along the myofibril axis compared the position of HSP27 in the I-bands (red dashed lines) with that of the remnant actin in the Z-disks after gelsolin treatment (black dashed line). Arrowheads, Z-disk. Bars, 5 µm.

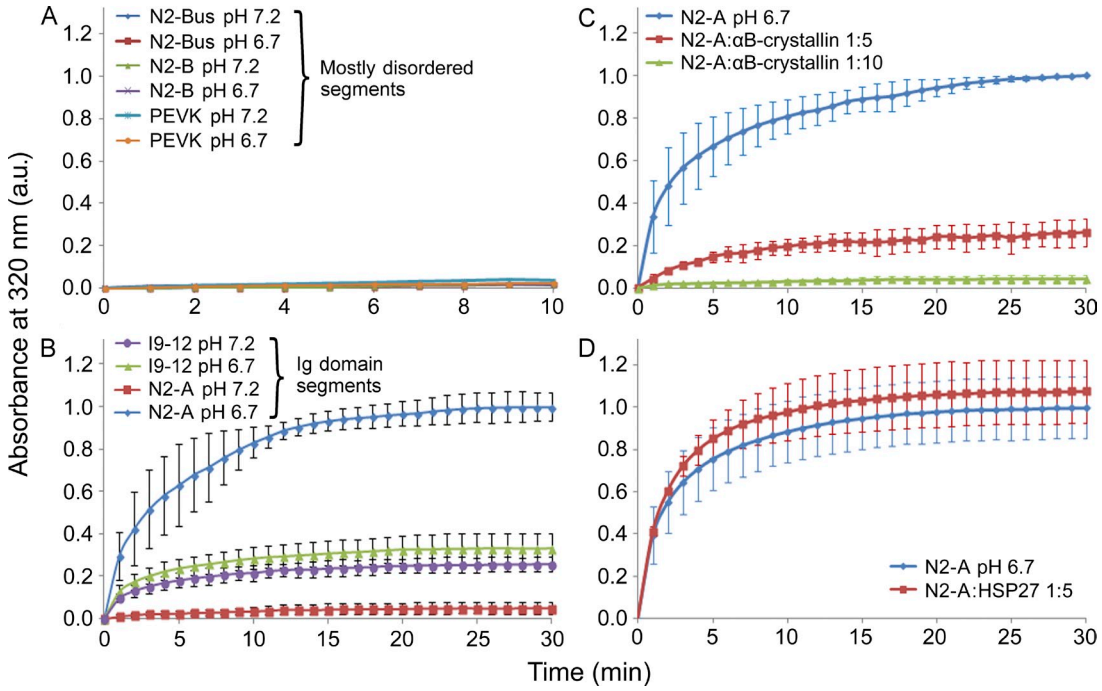

Figure 4. **pH-dependent aggregation of partially unfolded titin Ig constructs and protection by sHSPs.** Titin fragments were denatured in 8 mol/l of urea and then diluted 1:50 in neutral (pH 7.2) or acidic (pH 6.7) Tris/HCl buffer (30 mmol/l). Aggregation was determined by measuring the absorbance at 320 nm for up to 30 min. (A) Lack of aggregation of the mostly disordered segments, N2-Bus, N2-B, and PEVK, at normal and acidic pH. (B) Varied aggregation propensity of Ig-rich constructs, I9-12 and N2-A, at normal and acidic pH. (C) Protection by αB-crystallin against aggregation of the N2-A construct in pH 6.7 buffer at different N2-A/αB-crystallin molar ratios. (D) Lack of an anti-aggregation effect of HSP27 on N2-A at pH 6.7. All data were normalized to the absorbance value of N2-A at pH 6.7 at the 30-min time point and represent means ± SD (n = 6).

the stiff 3.0-MD N2B isoform, which is predicted to have already unfolded Ig domains at physiological SLs (Fig. 6 A and Fig. S4 B).

Confirming our expectations, fetal rat cardiomyocytes cultured in standard medium never revealed a sarcomeric (regular spacing) association with HSP27 and αB-crystallin, even though these sHSPs were highly abundant in the cytoplasm (Fig. 6 B). Various stressors applied to these cells, such as acidosis, contractile arrest, hypoxia, and cyclic/phasic stretch (10%), did not affect the distribution of sHSPs, which remained in the cytoplasm. Only upon treatment with the proteasome inhibitor MG132, which is known to boost sHSP levels, was sHSP binding to the Z-disk–I-band observed in some of the sarcomeres (Fig. S5). In contrast, in the adult rat cardiomyocytes, the two sHSPs always localized in the cytosol and at the Z-disk–I-band region (Fig. 6 C). Doublets, which indicate sHSP binding to the I-band, were clearly detectable at higher magnification (Fig. 6 C, insets). Some αB-crystallin was also observed at the M-band. These cells likely experienced mechanical strain and intracellular acidosis during the digestion procedure.

Stretch in the intact rat heart induces translocation of αB-crystallin to the elastic I-band

We investigated whether stretch in the isolated adult rat heart under adverse intracellular conditions, as induced by ex vivo perfusion with PBS, could trigger sHSP binding to the elastic I-bands. Hearts perfused for 30 min in the absence of stretch revealed cardiomyocytes with predominantly short sarcomeres (SL of ∼1.9 µm), which showed αB-crystallin exclusively at the Z-disk region (Fig. 7, left). However, a proportion of the myocytes in hearts perfused for 30 min in a high-stretch state showed greatly extended sarcomeres (up to SL of ∼2.6 µm). In those sarcomeres, αB-crystallin usually bound to both the Z-disk and the elastic I-band (Fig. 7, right). As the only difference, theoretically, between the two experimental conditions is the stretch state, the I-band binding of the sHSPs is presumed to directly follow the stretch-induced unfolding of titin Ig domains; the now-exposed hydrophobic sites on the titin springs facilitate protection by αB-crystallin, which is abundant in the cytosol of cardiomyocytes.

sHSPs translocate to the elastic I-bands in diseased cardiac and skeletal myocytes

To address the relevance of the sHSP–titin interaction in disease, we investigated the localization of HSP27 and αB-crystallin in heart samples obtained from healthy donors and patients with dilated cardiomyopathy (DCM) as well as in skeletal muscle biopsies (*Vastus lateralis*) from healthy subjects and patients with limb girdle muscular dystrophy type 2A (LGMD2A). In LGMD2A myocytes, endogenous HSP27 and αB-crystallin associated mainly with the elastic I-band region and rarely with the Z-disk (Fig. 8, A and B). Anti-HSP27 (Fig. 8 A) and anti–αB-crystallin antibodies (Fig. 8 B) showed marked staining on either side of the Z-disk; this staining pattern was always closer in distance to the Z-disk relative to the anti-PEVK staining representing titin sites (Fig. 8 C). The greater the degree of double band separation the greater that of sarcomere stretching, confirming the elastic

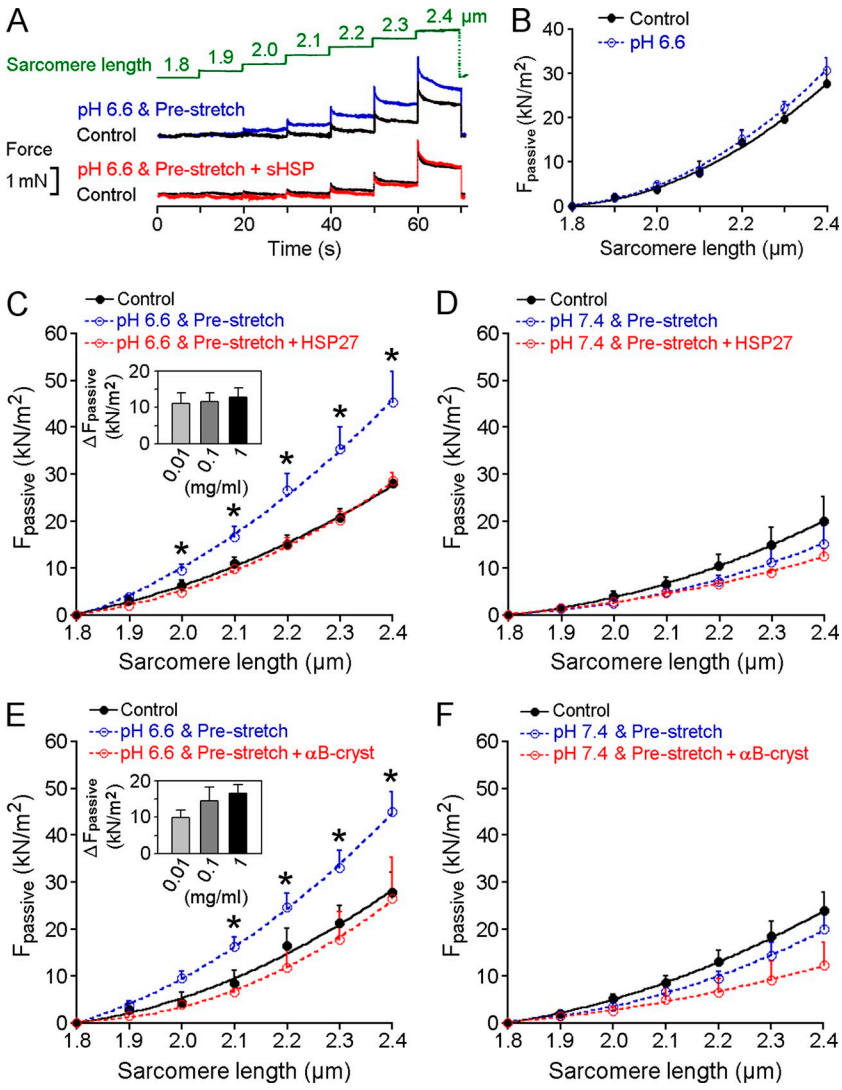

Figure 5. **The increase of passive tension in human skinned cardiomyocytes prestretched under acidic stress and protection by sHSPs.** (A) The original recordings for the force response to stepwise cell stretches in relaxing buffer, first at pH 7.4 (black curves) then at pH 6.6 after a 10-min prestretch to 2.6-µm SL in the absence (blue curve) or presence (red curve) of sHSP. (B) Passive tension ($F_{passive}$) at pH 7.4 (Control) and at pH 6.6. Cells were not prestretched. (C and E) The $F_{passive}$ at pH 7.4 (black curve) and at acidic pH after prestretch and hold to a 2.6-µm SL in the absence (blue curve) or presence (red curve) of sHSPs (0.1 mg/ml). Insets in C and E show the reduction of the $F_{passive}$ (at 2.2-µm SL) in pH 6.6 buffer using sHSP concentrations of 0.01, 0.1, or 1 mg/ml. (D and F) The $F_{passive}$ at pH 7.4 (black curve) and after a prestretch and hold to a 2.6-µm SL in the absence (blue curve) or presence (red curve) of sHSP (0.1 mg/ml) at normal pH 7.4. HSP27 (C and D) and αB-crystallin (E and F) were used. Data represent means ± SEM (n = 5–10 cells, derived from two human donor hearts); curves represent regression models of order 3; *, $P < 0.05$, prestretch (pH 6.6) versus prestretch + sHSP (pH 6.6).

nature of the sHSP binding region (Fig. 8 C). In contrast, healthy skeletal myocytes showed binding of HSP27 to the Z-disk (Fig. 8 A) and fuzzy cytosolic localization of αB-crystallin with faint Z-disk and M-band staining (Fig. 8 B). I-band staining was almost absent. In DCM hearts, many cardiomyocytes showed a double-banded pattern for sHSPs, indicative of I-band localization (Fig. 9, A and B). In these cases, HSP27 and αB-crystallin again localized between the Z-disk and the PEVK epitope, migrating away from the Z-disk during sarcomere stretch (Fig. 9 C). In control donor cardiomyocytes, HSP27 and αB-crystallin were abundant in the cytosol, especially at the Z-disk but not the I-band; anti-sHSP and anti-PEVK antibodies showed hardly any colocalization (Fig. 9, A and B).

Discussion

HSP27 and αB-crystallin have been investigated extensively in striated muscle, especially in regard to their induction during cardiac ischemia-reperfusion injury and their potential cardioprotective role. Here we provide new insight into the functional relevance of the translocation of these sHSPs to the sarcomeres, their primary binding sites in stressed myocytes. We demonstrated that HSP27 and αB-crystallin bound to titin spring elements and colocalized on I-band titin. The I-band association in sarcomeres was independent of actin filaments and enhanced by stretch. With increasing stretch, more titin Ig domains unfold, expose previously buried hydrophobic sites, potentially aggregate, and lose function. Our findings suggest that the unfolded Ig regions of the I-band titin, but not the intrinsically disordered segments, can aggregate to cause abnormally high titin-dependent myocyte stiffness. However, HSP27 and αB-crystallin translocated—likely promoted by acidic conditions—from the abundant pool of cytoplasmic sHSPs to the unfolded Ig regions, preventing their aggregation and maintaining functional (low-stiffness) titin. In line with this view, the sHSPs did not bind to cardiac sarcomeres that express the very compliant titin isoforms because the probability of Ig unfolding was very low even with stretching. In contrast, both sHSPs readily translocated to the I-bands of stretched sarcomeres that express relatively stiff titin. The two sHSPs were enriched at the elastic I-bands of human dystrophic muscles and failing hearts, suggesting a protective effect of sHSPs on titin springs in skeletal and cardiac muscle disease.

Previous studies of titin elasticity in situ and at the level of the single molecule demonstrated that the combined mechanical

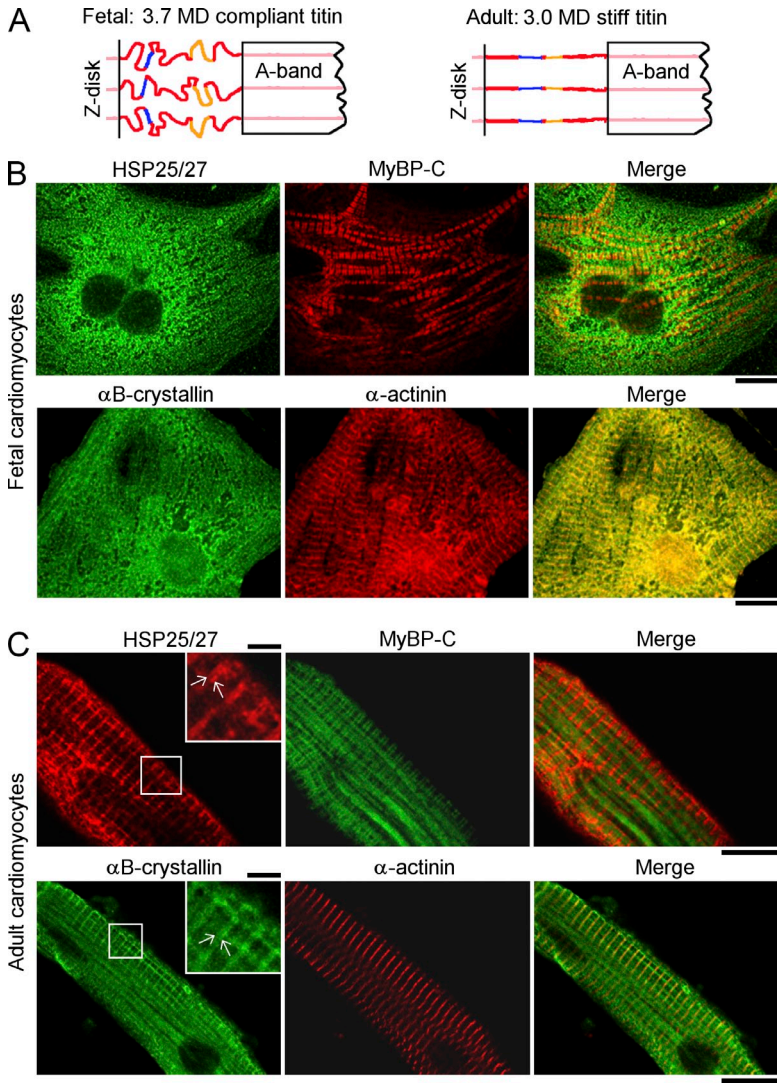

Figure 6. **HSP27 and αB-crystallin localize to the I-bands in adult but not fetal rat cardiomyocyte cultures.** (A) Schematics of the titin isoform sizes in fetal and adult rat cardiac sarcomeres. (B) Typical immunofluorescence images of fetal rat cardiomyocytes staining for HSP25/27 (secondary antibody: FITC-conjugated IgG) or endogenous αB-crystallin (secondary antibody: FITC-conjugated IgG; left) and counterstaining for A-band marker myosin-binding protein C (MyBP-C) (secondary antibody: Cy3-conjugated IgG) and Z-disk marker α-actinin (secondary antibody: Cy3-conjugated IgG), respectively. (C) Typical immunofluorescence images of adult rat cardiomyocytes staining for endogenous HSP25/27 (secondary antibody: Cy3-conjugated IgG) or endogenous αB-crystallin (secondary antibody: FITC-conjugated IgG) and counterstaining for A-band marker MyBP-C (secondary antibody: FITC-conjugated IgG) and Z-disk marker α-actinin (secondary antibody: Cy3-conjugated IgG), respectively. (insets) Higher-power images of the regions of interest indicated in the main panels. Arrows point to a doublet indicative of I-band binding of the sHSPs. Right panels show merged images. Rat HSP25 is homologous to human HSP27. Bars: (main) 10 µm; (insets) 2 µm.

properties of individual titin spring elements can explain the elasticity of titin in myocytes (Li et al., 2002). We supported this finding with evidence that the elastic elements traverse the I-band in a primarily monomeric state, whereas the dimeric state seldom existed. The monomeric behavior observed for the proximal Ig, N2-B, N2-A, and PEVK regions contrasted with the established hexameric state of the distal Ig region of titin (Fig. 10; Houmeida et al., 2008). Although distal Ig domains can unfold and aggregate in vitro (Wright et al., 2005; Marchetti et al., 2008; Somkuti et al., 2013), these domains are stabilized through their self-association in vivo (Houmeida et al., 2008). In contrast, the monomeric spring elements are more vulnerable to unfolding/aggregation and may bind preferentially to chaperones. Indeed, HSP27 and αB-crystallin did not interact with the self-associating distal Ig region near the A-band, as shown here and in Bullard et al. (2004), but rather with the elastic titin elements in between the Z-disk and the PEVK domain.

Only those titin spring segments predominantly or exclusively composed of Ig domains (proximal Ig/N2-A), but not the intrinsically disordered PEVK and N2-Bus (including the N2-Bus flanked by Ig domains, as in the N2-B construct), aggregated under conditions of partial denaturation. The primary strategy by which proteins escape aggregation is through folding, and Ig domains are protected from aggregation by their β-barrel folds. However, titin Ig domains mechanically unfold in stretched myofibrils (Minajeva et al., 2001). Overstretch is common under both physiological and pathological conditions, such as in skeletal muscle during exercise and in ischemic heart failure when myocyte death can lead to overstretch of adjacent myocytes. With overstretch, the probability of titin Ig unfolding increases greatly (Li et al., 2002). Although the unfolded Ig domains readily refold in vitro in the absence of chaperones (Rief et al., 1997; Linke and Grützner, 2008), they are at risk of aggregation under conditions of macromolecular crowding in the sarcomeres, requiring protection by sHSPs.

Intrinsically disordered proteins lack a well-defined secondary structure. They are resistant to aggregation through a variety of mechanisms, including a relatively high net charge and low hydrophobicity, low number of aggregating sequences, and evolutionary conservation of proline residues, which introduce constraints because of their distinctive cyclic structure (Wright et al., 2005; Monsellier and Chiti, 2007). The titin-PEVK domain is proline-rich with a higher net charge than other titin regions (Tskhovrebova and Trinick, 1997). The N2-Bus also

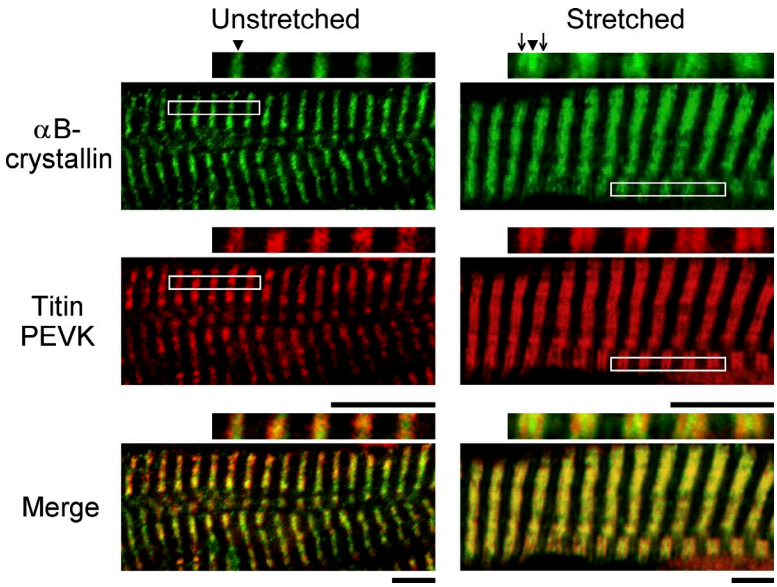

Figure 7. **Stretching of intact rat heart triggers the translocation of αB-crystallin to the elastic I-bands of cardiac sarcomeres.** Excised adult rat hearts were perfused with PBS for 30 min, either at low pressure to avoid sarcomere stretch (left) or at high pressure to obtain highly extended sarcomeres (right). Left ventricular sections were immunostained for endogenous αB-crystallin (secondary antibody: FITC-conjugated IgG; top) and counterstained for PEVK titin (secondary antibody: Cy3-conjugated IgG; middle). The representative images for each condition are shown. Higher-power images of the region of interest indicated are shown above the main panels. Arrowheads point to the Z-disk localization of αB-crystallin and arrows to I-band localization. Bottom panels show merged images. Bars, 5 µm.

contains more proline residues and an above average net charge than a typical titin Ig domain. Supporting our experimental results, the TANGO algorithm (Linding et al., 2004) predicted lack of aggregation propensity for the PEVK domain, and the aggregation tendency of N2-Bus, albeit much higher compared with PEVK, was predicted to be lower than that of unfolded Ig segments. Consistent with our findings, aggregation of thermally unfolded (distal) titin Ig domains, excluding PEVK, was recently demonstrated in vitro (Somkuti et al., 2013). In summary, the disordered N2-Bus and PEVK segments have intrinsic properties that help prevent aggregation, potentially precluding the protection provided by sHSPs.

Intrinsically disordered proteins generally exhibit no preference for chaperone binding in vivo (Hegyi and Tompa, 2008). We showed here that the PEVK domain did not interact with HSP27, and others have shown little to no interaction with αB-crystallin (Bullard et al., 2004). The fact that PEVK is not recognized by sHSPs as "unfolded" underscores the specialized nature of this sequence, which is not merely a canonical unfolded peptide (Linke et al., 1998; Leake et al., 2004). N2-Bus, the other large sequence insertion in I-band titin, also demonstrates unique structural organization (Leake et al., 2006), but this domain, although not undergoing aggregation, did associate with HSP27 and αB-crystallin. Because the N2-Bus is intrinsically disordered, mechanical unfolding of this region is probably not required for sHSP binding. Consistent with this view was our observation that exogenous sHSPs bound to unstretched isolated cardiac myofibrils, whereas they showed little (αB-crystallin) to no (HSP27) binding to unstretched skeletal myofibrils, which do not express N2-Bus. In an attempt to find a possible regulatory mechanism for the interaction between N2-Bus and HSP27, we generated HSP27 phosphomimicking mutants because the phosphorylation of sHSPs has occasionally (though not consistently) been reported to promote client binding (Mymrikov et al., 2011). However, we did not observe altered binding of these mutants to N2-Bus compared with wild-type HSP27, suggesting this interaction may be phosphorylation independent. We speculate that sHSP binding to the N2-Bus, regardless of the stimulus, plays a role in promoting the formation of protein complexes, a function proposed for several other chaperones (Hegyi and Tompa, 2008; Donlin et al., 2012). The N2-Bus interacts with the four-and-a-half-LIM domain family of proteins, which target protein kinases to the N2-Bus (Lange et al., 2002; Sheikh et al., 2008). The sHSPs may help regulate the formation of these macromolecular complexes, perhaps in conjunction with other chaperones/cochaperones. A similar scenario was recently suggested for complexes involving the Z-disk protein filamin (Ulbricht et al., 2013).

Aggregation of unfolded titin Ig regions in the sarcomere and sHSP-mediated protection from aggregation have important consequences for the mechanical properties of cardiac and skeletal myocytes. Although αB-crystallin increased the mechanical stability of proximal and distal Ig domains as well as the N2-Bus, according to single-molecule atomic force spectroscopy experiments (Bullard et al., 2004; Zhu et al., 2009), isolated human cardiomyocytes did not become stiffer in the presence of sHSPs. Instead, under conditions promoting titin aggregation (prestretch and acidic pH), the passive tension was abnormally high and αB-crystallin/HSP27 suppressed this increase in stiffness. Thus, the prevention of titin aggregation by sHSPs more than compensated for their domain-stabilization effect: the overall mechanical effect of sHSP binding to I-band titin in stressed sarcomeres decreased the stiffness.

Acidic buffer together with prestretch were prerequisites for the development of abnormally high cardiomyocyte stiffness and sHSP mechanical effects. Acidosis is known to promote the aggregation of unfolded proteins and to boost sHSP binding and client protection (Bennardini et al., 1992; Barbato et al., 1996; Ehrnsperger et al., 1999; Chernik et al., 2004). Acidosis alone is sufficient to trigger αB-crystallin binding to cardiomyofibrils (Barbato et al., 1996) and to increase the chaperone activity of HSP27 (Chernik et al., 2004). In our in vitro assays, acidic conditions marginally promoted aggregation of the proximal Ig domains I9-12 and strongly promoted that of N2-A; αB-crystallin fully protected

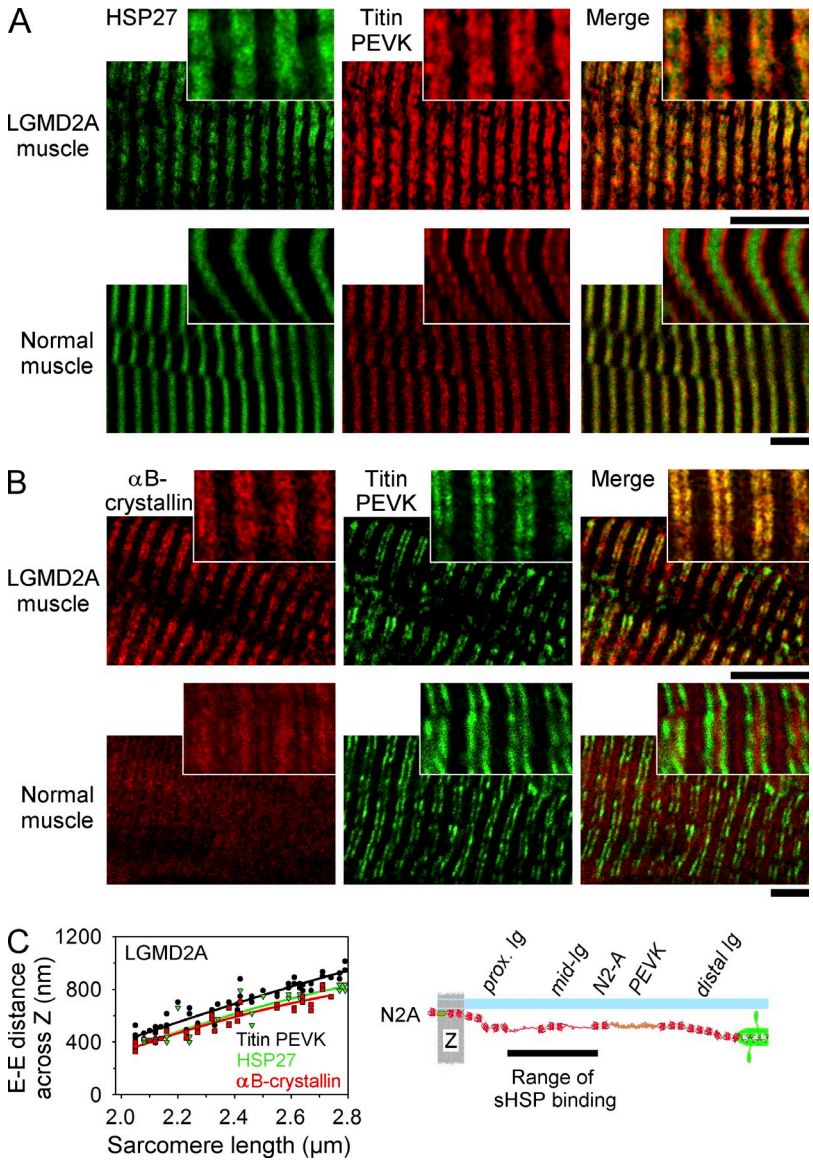

Figure 8. **Binding of sHSPs to the elastic I-bands in human dystrophic skeletal muscle.** (A and B) Representative immunofluorescence images of sectioned muscle biopsies comparing tissue from healthy subjects with that from LGMD2A patients. (A) Immunostaining for endogenous HSP27 (secondary antibody: FITC-conjugated IgG; left) and counterstaining for PEVK titin (secondary antibody: Cy3-conjugated IgG; middle). (B) Immunostaining for endogenous αB-crystallin (secondary antibody: Cy3-conjugated IgG; left) and counterstaining for PEVK titin (secondary antibody: FITC-conjugated IgG; middle). Right panels show merged images. (insets) Higher-power images of sections differing from those shown in the respective main panels. Bars, 5 µm. (C) Relative I-band positions of endogenous sHSPs and PEVK at different SLs in myocytes from LGMD2A patients (left). Each data point represents an epitope–epitope (E-E) distance value measured across the Z-disk. Regression curves are of order 2. The right panel illustrates the range of sHSP binding locations on titin.

N2-A from aggregation when present in 10-fold molar excess. Somewhat surprisingly, HSP27 did not prevent N2-A aggregation, even though it protected from abnormally high cardiomyocyte stiffness. However, HSP27 (as well as αB-crystallin) presumably protects titin domains that were not tested here against aggregation, good candidates being the proximal and middle Ig domains according to the I-band position of the sHSPs in stressed myocytes. Moreover, HSP27 can exchange subunits with αB-crystallin and form both homo- and heterooligomers (Sun and MacRae, 2005). Because the two sHSPs were detected at the same I-band titin positions, heterooligomerization cannot be excluded. HSP27 is known to stabilize αB-crystallin (Fu and Liang, 2003), such that the presence of HSP27 could enhance binding of αB-crystallin to titin. In any case, the 6.6–6.7 pH range at which titin Ig domains aggregated and sHSPs exerted their protective effect has been observed in myocytes of metabolically stressed muscle (Khong et al., 2001) and in cardiomyocytes of acute ischemic hearts (Vaughan-Jones et al., 2009), together with the induction of sHSPs. Acidic conditions impair the generation of active tension in skeletal muscle and myocardium (Orchard and Kentish, 1990) and can also increase passive tension (Berger et al., 1999; Miyake et al., 2003). In principle, active contraction may be enhanced by sHSP protective effects on actin, troponin, or myosin. However, the preferential association of sHSPs with the elastic I-band in stressed myocytes indicates that titin is the primary sHSP client. The main role played by sHSPs may thus be the maintenance of low passive stiffness. In line with this view, contractile parameters were unaltered but passive stiffness pathologically elevated during ischemia in mouse hearts deficient in αB-crystallin and HSPB2, compared with ischemic wild-type mouse hearts (Golenhofen et al., 2006). Thus, sHSPs have an unappreciated role in protecting the myocardium from diastolic mechanical dysfunction, such as that during ischemia-reperfusion damage.

The protective effect of sHSPs on titin-based passive stiffness may also be present in other types of heart and skeletal muscle diseases. During heart failure in patients and in animal models, and in subjects with dystrophic muscles, sHSPs tended to be up-regulated in myocytes and translocated to the myofilaments

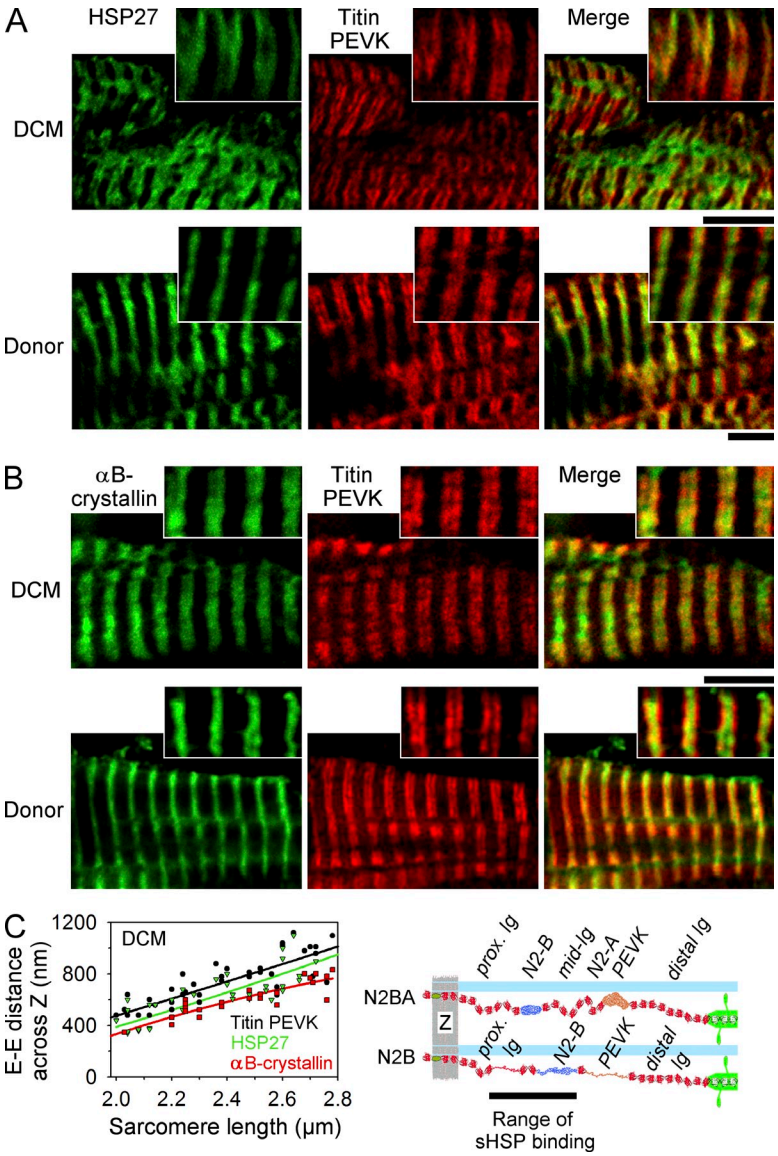

Figure 9. **Binding of sHSPs to the elastic I-bands in failing human heart.** (A and B) Representative immunofluorescence images of sectioned myocardial tissue from control donor hearts and failing hearts with DCM. (A) Immunostaining for endogenous HSP27 (secondary antibody: FITC-conjugated IgG; left) and counterstaining for PEVK titin (secondary antibody: Cy3-conjugated IgG; middle). (B) Immunostaining for endogenous αB-crystallin (secondary antibody: FITC-conjugated IgG; left) and counterstaining for PEVK titin (secondary antibody: Cy3-conjugated IgG; middle). Right panels show merged images. (insets) Higher-power images from sections differing from those shown in the respective main panels. Bars, 5 μm. (C) Relative I-band positions of endogenous sHSP and PEVK at different SLs in DCM cardiomyocytes (left). Each data point represents an epitope–epitope (E-E) distance value measured across the Z-disk. Regression curves are of order 2. The right panel illustrates the range of sHSP binding locations on titin.

(Knowlton et al., 1998; Fischer et al., 2002; Dohke et al., 2006; Li et al., 2012; Kley et al., 2012). We showed that αB-crystallin and HSP27 were targeted to the cytosol and/or sarcomeric Z-disks in the normal human heart and skeletal muscles. However, in skeletal myocytes of LGMD2A patients and in cardiomyocytes of failing human DCM hearts, a significant portion of the sHSP pool was found in the elastic I-band region colocalizing with the titin springs. Failing hearts often show pathologically altered cardiomyocyte passive stiffness caused by isoform switching and aberrant phosphorylation of titin (Linke and Krüger, 2010); degenerating skeletal myofibers also display abnormal stiffness (Olsson et al., 2006). Our study has revealed additional stiffness-modulating processes common to diseased myocytes involving titin aggregation and its protection by sHSPs.

In summary, this work established a novel role for αB-crystallin and HSP27 in myocytes involving the protection of unfolded titin Ig domains from aggregation in the presence of acidosis. Thus, sHSPs may help prevent titin spring loss of function and the development of abnormally high passive stiffness in myocytes. This protective mechanism is operative in cardiomyocytes of human failing hearts and in skeletal myocytes of muscular dystrophy, in which it can be induced by overstretch and acidic stress. Even in healthy skeletal myocytes during exercise, such could be an early repair mechanism for titin to preserve the protein's elasticity and additional roles in mechanotransduction and mechanosensation. More generally, the concept of aggregation-induced mechanical stiffening under adverse intracellular conditions and its protection by sHSPs may apply to other mechanical proteins in several cell types. We conclude that in muscle/myocardium, chaperone-mediated protection of titin springs is an effective stress mechanism that maintains low passive myocyte stiffness and preserves diastolic heart function.

Materials and methods

Recombinant constructs and site-directed mutagenesis

Fragments of human I-band titin were expressed in *Escherichia coli* BL21De3 pLys cells (New England Biolabs, Inc.) and purified using the GST-Fusion System (GE Healthcare). Each construct was expressed twice at

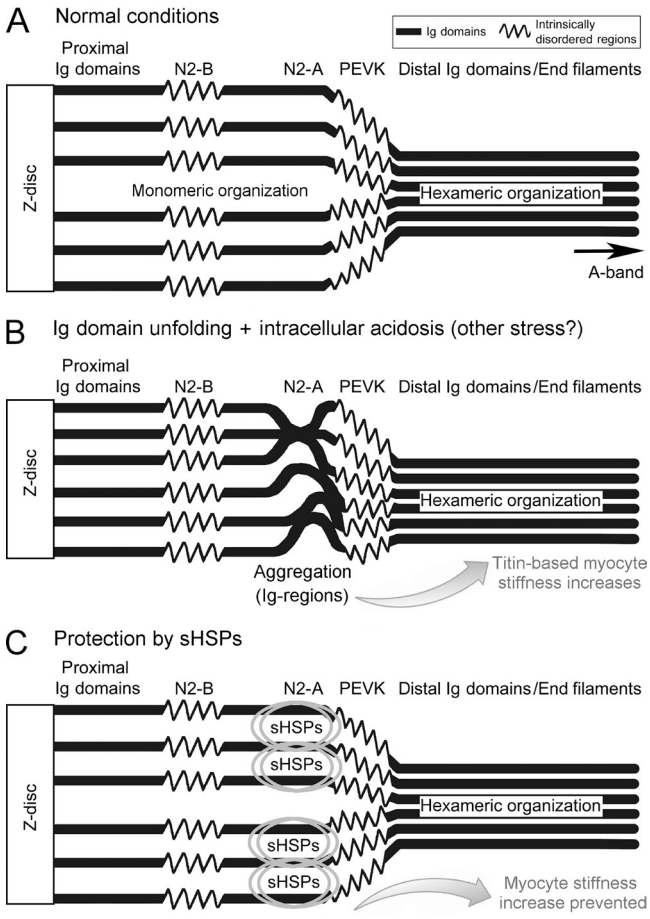

Figure 10. **The proposed titin organization in the sarcomeric I-band under normal and stress conditions and the protective effects of sHSPs.** (A) Elastic titin filaments normally traverse the I-band in a monomeric state, except in the distal Ig region where they form hexamers (Houmeida et al., 2008). (B) Unfolding of I-band Ig domains together with acidic stress may cause increases in titin aggregation and myocyte stiffness. The mechanically more stable, self-associating, distal Ig domains likely do not unfold. Intrinsically disordered titin regions (N2-Bus and PEVK) do not aggregate. (C) Association of sHSPs with unfolded Ig domains in a region between the Z-disk–I-band junction and PEVK protects against titin aggregation and helps prevent abnormal myocyte stiffening.

minimum. The generated constructs were as follows: Z7-I1 (Z-disk–I-band junction), I9-12 (proximal Ig domains), I24/25 (Ig domains N-terminal to N2-Bus), N2-Bus (large unique sequence of N2-B region), I26 (Ig domain C-terminal to N2-Bus), entire N2-B region (I24/25 + N2-Bus + I26 of exon 49), N2A (four Ig domains and intervening sequences of exons 102–109), and the constitutively expressed PEVK segment (exons 219–225). The human titin sequence was derived from the NCBI accession numbers nm_003319 (N2B isoform) and nm_133378 (N2A isoform). Titin domains were numbered according to Bang et al. (2001). Recombinant human αB-crystallin (NCBI accession no. nm_001885) and HSP27 (NCBI accession no. nm_001540) proteins each were generated using the same expression and purification system. In the cardiomyocyte mechanical studies, we also used commercial recombinant human HSP27 (ab48740; Abcam) and αB-crystallin (ab48779; Abcam). All constructs were verified by sequencing. Primer sequences are listed in Table S1.

To mimic constitutive phosphorylation of HSP27, serine residues 15, 78, and 82 were mutated to aspartate. Site-directed mutagenesis was performed using a two-step PCR reaction (Hamdani et al., 2013), as described in Table S1. Titin fragments were ligated into the pGEX4T2 expression vector and transformed into competent *E. coli* XL1-blue (Agilent Technologies) or BL21De3 pLys cells (New England Biolabs, Inc.). All constructs were validated by sequencing. Fragments were expressed as GST fusion proteins using 0.2 mmol/l isopropyl-β-D-thiogalactopyranoside and purified using glutathione affinity chromatography. The GST tag was cleaved with thrombin (10 U) and removed from solution using paraaminobenzamidine sepharose beads.

Ion-exchange chromatography

This technique was used to further purify constructs after the GST affinity purification protocol using 1-ml RESOURCE Q columns (GE Healthcare).

Analytical ultracentrifugation

Sedimentation-velocity centrifugation was performed in an XL-A centrifuge (Beckman Coulter) equipped with absorption optics and a four-hole titanium rotor. Samples (300–400 µl) were loaded into standard aluminum double-sector centerpieces with quartz windows and spun at 45,000–52,000 rpm at 20°C. Purified titin constructs were suspended in 30 mmol/l Tris-HCl, pH 7.2, and 50 mmol/l KCl buffer in the following concentrations: N2-Bus, 9.5 or 13 µmol/l; N2-B, 3.5 or 5 µmol/l; N2-A, 9.5 µmol/l; and PEVK, 63 µmol/l. Radial scans were recorded at a 0.003-cm resolution every ∼1.5 min. The detection wavelength was 280 nm (N2-Bus/N2-B/N2-A) or 220 nm (PEVK). Data analysis was performed with SedFit, version 11.9 (National Institutes of Health), which estimates the mixture of macromolecular species as a system of noninteracting species with the weight-averaged frictional coefficient ratio (f/f_0). Parameters were set as follows: *s*-value resolution, 200; *s*-value range, 0–20 S; confidence interval, 0.95. Time- and radial-invariant noise was calculated; the bottom of the cell and the baseline were fitted. The frictional ratio was floated for the calculation of c(s) and c(M) distributions. Hydrodynamic parameters were corrected for buffer density, viscosity, and partial specific volume, as implemented in SEDNTERP, version 1.09. The partial specific volumes at 20°C were calculated as 0.7347 $cm^3\ g^{-1}$ for N2-B and N2-Bus, 0.7323 $cm^3\ g^{-1}$ for N2-A, and 0.7589 $cm^3\ g^{-1}$ for PEVK, based on the amino acid composition. The mass density of the buffer was calculated as 1.0015 g cm^{-3} and the viscosity as 1.0059 cp at 20°C. Experiments were run at least twice per construct with similar results (only one dataset shown).

Size-exclusion chromatography

Gel-filtration assays were performed using the ÄKTAFPLC on a Superose 12 column (GE Healthcare) in 20 mmol/l Tris/HCl, pH 7.2, and 50 mmol/l NaCl. Proteins were added in a 500-µl super loop and separated by a flow rate of 500 µl/min. The eluate was collected in 500-µl fractions. Eluted proteins were detected at 280 nm (I9-12 construct) or 220 nm (PEVK construct), and the elution profiles (absorption versus elution volume) were recorded. For size determination, results were compared with those obtained with a reference protein of known size (66 kD BSA). Experiments were run at least three times for each construct with similar results (only one dataset shown).

GST pulldown assay

Binding assays were performed at 4°C using recombinant fragments of human I-band titin and human αB-crystallin or HSP27 protein according to standard protocols (Donlin et al., 2012). In brief, the titin fragment or sHSP protein was immobilized on GSH-sepharose beads and incubated with supernatant containing the potential interaction partner. The beads were washed four times, and the interaction was detected by Western blotting with 1-h incubations of anti-titin or anti-sHSP antibodies (dilution 1:1,000) and 1-h incubations of horseradish peroxidase–conjugated anti-rabbit or anti-mouse secondary antibodies (dilution 1:10,000). Detection was performed using the LS 4000 imager (Fujifilm). Each binding test was repeated at least twice.

Yeast two-hybrid assay

Using an established protocol for direct binding assays in yeast (Donlin et al., 2012), human titin N2-Bus (bait) was cloned into a pGBKT7 vector and transformed into the yeast strain Y187 (Agilent Techonologies). HSP27 or αB-crystallin (prey) was cloned into a pACT2 vector and transformed into the yeast strain AH109 (Agilent Techonologies) using electroporation. Strains were crossbred and plated on triple drop-out plates. To eliminate false-positive interactions, yeast colonies were tested for active β-galactosidase using an X-Gal filter lift assay. In the presence of X-Gal, positive clones turned blue and were analyzed using PCR.

Measurements of mechanical stretch, fluorescence staining, and force in single myofibrils

Myofibrils were isolated from thawed human donor heart, rabbit psoas, or rabbit cardiac muscle tissues following our established protocols (Linke et al., 1999; Neagoe et al., 2002). In brief, single myofibrils were stretched in relaxing buffer (1 mmol/l of free Mg, 100 mmol/l KCl, 2 mmol/l EGTA, 4 mmol/l Mg-ATP, and 10 mmol/l imidazole, pH 7.0) at room temperature using an inverted microscope (Axiovert 135; Carl Zeiss) with a pair of micromanipulators. Non-stretched and stretched samples were incubated

for 30 min with recombinant αB-crystallin or HSP27 at a concentration of 0.2 mg/ml in relaxing buffer; this concentration is within the range reported for cardiac and skeletal muscle cells (Inaguma et al., 1995; Larkins et al., 2012). After washing away unbound sHSP, myofibrils were incubated with anti–αB-crystallin or anti-HSP27 antibodies (1:250 dilution) for 30 min, followed by Cy3-conjugated secondary antibodies (1:500) for 30 min. In control experiments, myofibrils were incubated with secondary antibodies alone or with recombinant GFP (0.2 mg/ml). Human cardiomyofibrils were treated before antibody incubation with sHSPs and antibodies with a Ca^{2+}-independent gelsolin fragment to extract sarcomeric actin filaments (and their associated regulatory proteins; e.g., troponin). Extraction was verified by actin staining using rhodamine-phalloidin. Fluorescence measurements and the corresponding phase-contrast images were obtained using a Plan-Neofluar 100× oil-immersion objective (NA 1.3; Carl Zeiss), a color 3CCD camera (DXC 930P; Sony), and ImageJ acquisition software (National Institutes of Health). Images were filtered using the built-in "Soften" command of ImageJ. The positions of the fluorescence signals were determined using the measurement tool of ImageJ. The staining results for each experimental condition were verified at least once.

Single rabbit psoas and cardiac myofibrils were used for measurements of dynamic stiffness in relaxing buffer at room temperature. Slightly stretched samples were oscillated using a piezo motor at an amplitude of 20 nm per half-sarcomere and a frequency of 20 Hz, and the oscillatory force response was recorded over a 1-s period using a custom-designed force transducer (Linke et al., 1998, 1999). The mean force-oscillation amplitude was used as a measure of the dynamic stiffness. Measurements were performed in relaxing solutions of varying pH (7.4, 7.0, 6.6, and 5.9), and in the case of the rabbit psoas myofibrils, after treatment with the actin-severing, Ca^{2+}-independent gelsolin fragment for 20 min.

Prediction of unfolded protein aggregation

TANGO (http://tango.crg.es/protected/academic/calculation.jsp), an algorithm that predicts the regions subjected to aggregation in unfolded polypeptide chains (Linding et al., 2004), was used to predict the aggregation tendency of the I-band titin unfolded regions. The following parameters and conditions were selected: no N- and C-terminal protection, pH 7.0, 300°K temperature, and 0.2 mol/l ionic strength. The relative propensity for β aggregation was plotted for each amino acid of the respective sequence.

In vitro aggregation assays

Recombinant titin fragments (1 µmol/l final concentration) were exposed to conditions promoting partial denaturation (8 mol/l urea followed by dilution in 30 mmol/l Tris/HCl, pH 7.2 or 6.7, and 50 mmol/l KCl buffer). Many proteins do not refold efficiently after dilution with denaturants but rather form misfolded aggregates. As a measure of aggregation, the absorbance was recorded at 320 nm for up to 30 min. Rhodanese protein aggregation, a known positive control (Martin et al., 1991), was measured under the same conditions and found to be similar to N2-A-titin aggregation in terms of absolute absorbance values. In experiments with the aggregating N2-A construct, we added recombinant human αB-crystallin or HSP27 to Tris buffer at a final concentration of 5 or 10 µmol/l. Experiments were performed at room temperature and run multiple times per condition.

Cardiomyocyte force measurement

Demembranated single human cardiomyocytes were prepared from donor heart tissue as described previously (Hamdani et al., 2013). In brief, samples were thawed in relaxing buffer (1 mmol/l of free Mg, 100 mmol/l KCl, 2 mmol/l EGTA, 4 mmol/l Mg-ATP, and 10 mmol/l imidazole, pH 7.4), mechanically disrupted, and incubated for 5 min in relaxing solution supplemented with 0.5% Triton X-100. The cell suspension was washed five times in relaxing solution. A single cardiomyocyte was attached in relaxing buffer between a force transducer and a micromotor on the stage of an Axiovert 135 microscope (Plan-Neofluar 40× objective, NA 0.75) as part of the Permeabilized Myocyte Test System (1600A; force transducer 403A; Aurora Scientific). The force response to the stepwise cell stretches ($F_{passive}$) was recorded at room temperature in relaxing buffer for a range of SLs (1.8–2.4 µm). The experimental protocol consisted of recording the $F_{passive}$, first in normal pH 7.4 buffer (control) and again after the cell was stretched to ∼2.6-µm SL, incubated in pH 6.6 relaxing buffer, and held in the stretched state for 10–15 min (prestretch). The myocyte was returned to the slack length and rested for several minutes before recording the $F_{passive}$ in the low pH buffer. Alternatively, the pH 6.6 buffer was supplemented with recombinant human αB-crystallin or HSP27 at three different concentrations (0.01, 0.1, or 1 mg/ml), which cover their reported expression range in cardiac and skeletal myocytes (Inaguma et al., 1995; Larkins et al., 2012), and the $F_{passive}$ was measured in the presence of the sHSPs. In other experiments, the protocol was modified to either omit the prestretch step or to use normal pH 7.4 relaxing buffer throughout. Force values were normalized to the myocyte cross-sectional area calculated from the major and minor diameters of the cell, assuming an oval shape. SL was measured in the experiments using the built-in features of the setup (Aurora Scientific). To test cell viability, each cardiomyocyte was additionally transferred from a relaxing to maximally activating solution (pCa 4.5). Once the steady-state force was reached, the cell was quickly released to 80% of its original length to determine the baseline force. Only cells that developed active forces >20 kN/m^2 were included in the analysis.

Induction of stretch in rat heart

Adult rat hearts were quickly excised and the aorta was tied with a thread to a cannula connected to a perfusion system. Retrograde perfusion with nonoxygenated PBS (20°C) was performed using a peristaltic pump generating pressure sufficient to maintain the left ventricle in a well-stretched state. Alternatively, the aorta was connected to the cannula only loosely to allow ample perfusion of the left ventricle at low pressure and no stretch. Total perfusion time was 30 min. Subsequently, the heart was immediately fixed using a solution containing 4% paraformaldehyde and 15% picric acid. Two left ventricles/experimental condition were prepared for immunohistochemistry.

Human tissues

We obtained nonfailing donor heart tissue and end-stage failing left ventricular tissue from patients with ischemic DCM, as well as *Vastus lateralis* muscle biopsies from healthy human subjects and patients with LGMD2A, who have a mutation in the CAPN3 gene encoding the calpain 3 protease. Tissue was obtained from two different subjects per condition. Human heart and muscle biopsy collections were in accordance with national guidelines. This study conformed to the principles outlined in the Declaration of Helsinki and was approved by the Ethics Committee at Ruhr University Bochum (entries 3447–09 and 3483–09, respectively).

Immunohistochemistry

Heart and muscle tissues were prepared for indirect immunofluorescence using standard protocols. In brief, stretched or unstretched samples were fixed with 4% formaldehyde and embedded in paraffin, and 5-µm-thick sections were prepared. Sections were washed twice with PBS and incubated in blocking buffer (0.5% Triton X-100 and 5% goat serum in PBS) for 1 h. Antibodies were diluted in staining buffer (0.5% goat serum in PBS), the primary antibodies were applied overnight at 4°C, and the secondary antibodies were applied for 2 h at room temperature, with three washes between incubations. Antibody incubations were performed in the dark under agitation. Sections were embedded in Mowiol, and microscopic images were recorded at room temperature using a confocal laser scanning microscope (A1; Nikon) equipped with a CFI Plan Apo 100× oil-immersion objective (NA 1.4) and NIS-Elements software (Nikon). The primary antibodies used were anti-HSP27 (1:250 dilution in PBS; SMC161 5D12; StressMarq), anti-HSP27 (1:200; SR B800; MBL), anti–αB-crystallin (1:250; SMC 165 3A10; StressMarq), anti–αB-crystallin (1:400; SR 223F; MBL), anti-titin PEVK (1:200; 9D10; Hybridoma Bank), and anti-titin PEVK (1:500; custom-made, affinity-purified; Eurogentec; Hamdani et al., 2013). Secondary antibodies were Cy3- or FITC-conjugated IgG (1:400; Rockland). Recorded myocyte images were filtered using the "Soften" command in ImageJ. For some images, we measured the nearest distance across the sarcomeric Z-disk between the mean epitope positions of αB-crystallin, HSP27, and PEVK using ImageJ, as described previously (Linke et al., 1999). The distance between epitopes was plotted against the SL, and data points for each antibody type were fitted by a regression model of order 2.

Primary cultures of fetal and adult rat cardiomyocytes

Hearts were obtained from day 18 embryos of pregnant adult Sprague-Dawley rats. Animals were anaesthetized by isoflurane and euthanized by decapitation. Cells were isolated using enzymatic digestion, the fibroblasts removed by a 60-min preplating step, and cardiomyocytes cultured at 37°C on gelatin-coated coverslips (Krüger et al., 2008). The day after plating, a portion of the fetal cells was treated with the 26S proteasome inhibitor MG132 (5 µM) for 2 h. Other cell groups were perturbed by various stressors, including hypoxia, lactic acid (100 mmol/l; 2 h), contractile arrest (high KCl; Krüger et al., 2008), or 10% cyclic or static stretch using the Flexcell stretcher apparatus (Dunn Labortechnik). Cells were fixed in 3% paraformaldehyde (20 min) and stained with the respective antibodies using standard protocols. Cardiomyocytes were also isolated from adult (3-mo-old) rat hearts by enzymatic digestion as

described previously (Kienitz et al., 2011). In brief, Wistar Kyoto rats (~200 g) were anesthetized by intravenous injection of urethane (1 g/kg) and killed following protocols approved by the animal welfare regulation local authorities in accordance with the guidelines of the European Community (86/609/EEC). Hearts were perfused in a modified Langendorff apparatus under constant flow and sterile conditions; left ventricular myocytes were prepared by enzymatic extraction. Cells were cultured overnight on laminin-coated cover glasses at 37°C in M199 medium (Life Technologies) containing 5% fetal calf serum. Before plating, the serum was removed with several washes of serum-free culture medium (Hepes-buffered M199). Cells were examined between the second and fifth days of culture. Cells were fixed in 3% paraformaldehyde for 20 min at 20°C and stained with antibodies.

For indirect immunofluorescence, cultured cardiomyocytes were incubated for 1 h at room temperature with primary antibodies against HSP25/27 (ProteinTech; dilution 1:250 in PBS) or αB-crystallin (1:500; MLB Antibodies) and counterstained with antibodies against α-actinin (1:500; Sigma-Aldrich) or myosin-binding protein C (Witt et al., 2001), followed by staining for 1 h with FITC- (Sigma-Aldrich) or Cy3-conjugated (Rockland) secondary antibodies (1:500). Images were recorded using an Axiovert 200 microscope (Plan-Neofluar 100× oil-immersion objective, NA 1.3; Carl Zeiss) in epifluorescence mode using a color 3CCD camera (DXC 930P) and ImageJ acquisition software. Images were filtered using the built-in "Soften" command of ImageJ. The epitope positions of endogenous HSP27 and αB-crystallin in sarcomeres were determined in relation to that of the Z-disk or A-band markers. At least 10 different cells per experimental condition were included in the analysis.

Statistics

The statistical significance of the data were determined using the paired Student's *t* test (Prism 5; GraphPad). A value of $P < 0.05$ was taken to indicate statistical significance.

Online supplemental material

Fig. S1 shows additional tests for interaction between N2-Bus and sHSPs. Fig. S2 shows the β aggregation tendency of titin regions predicted by TANGO. Fig. S3 shows control measurements of dynamic myofibril stiffness at varying pH values. Fig. S4 shows predictions of force/titin based on entropic elasticity theory. Fig. S5 shows the partial translocation of sHSPs to the Z-disk–I-band region of cultured fetal rat cardiomyocytes after proteasome inhibition. Table S1 lists the human titin primer sequences used in this study. Online supplemental material is available at http://www.jcb.org/cgi/content/full/jcb.201306077/DC1.

We thank Anna Eliane Müller for assistance with the adult cell cultures, Judith Krysiak for the yeast two-hybrid data, and Wolfgang Obermann for advice on the protein aggregation assays.

The study was funded by grants from the Deutsche Forschungsgemeinschaft to W.A. Linke (Li 690/7-2; SFB1002, TPB3).

The authors have no conflicting financial interests.

Submitted: 14 June 2013
Accepted: 3 December 2013

References

Bang, M.L., T. Centner, F. Fornoff, A.J. Geach, M. Gotthardt, M. McNabb, C.C. Witt, D. Labeit, C.C. Gregorio, H. Granzier, and S. Labeit. 2001. The complete gene sequence of titin, expression of an unusual approximately 700-kDa titin isoform, and its interaction with obscurin identify a novel Z-line to I-band linking system. *Circ. Res.* 89:1065–1072. http://dx.doi.org/10.1161/hh2301.100981

Barbato, R., R. Menabò, P. Dainese, E. Carafoli, S. Schiaffino, and F. Di Lisa. 1996. Binding of cytosolic proteins to myofibrils in ischemic rat hearts. *Circ. Res.* 78:821–828. http://dx.doi.org/10.1161/01.RES.78.5.821

Benjamin, I.J., and D.R. McMillan. 1998. Stress (heat shock) proteins: molecular chaperones in cardiovascular biology and disease. *Circ. Res.* 83:117–132. http://dx.doi.org/10.1161/01.RES.83.2.117

Bennardini, F., A. Wrzosek, and M. Chiesi. 1992. Alpha B-crystallin in cardiac tissue. Association with actin and desmin filaments. *Circ. Res.* 71:288–294. http://dx.doi.org/10.1161/01.RES.71.2.288

Berger, D.S., S.K. Fellner, K.A. Robinson, K. Vlasica, I.E. Godoy, and S.G. Shroff. 1999. Disparate effects of three types of extracellular acidosis on left ventricular function. *Am. J. Physiol.* 276:H582–H594.

Bullard, B., C. Ferguson, A. Minajeva, M.C. Leake, M. Gautel, D. Labeit, L. Ding, S. Labeit, J. Horwitz, K.R. Leonard, and W.A. Linke. 2004. Association of the chaperone alphaB-crystallin with titin in heart muscle. *J. Biol. Chem.* 279:7917–7924. http://dx.doi.org/10.1074/jbc.M307473200

Chernik, I.S., O.O. Panasenko, Y. Li, S.B. Marston, and N.B. Gusev. 2004. pH-induced changes of the structure of small heat shock proteins with molecular mass 24/27 kDa (HspB1). *Biochem. Biophys. Res. Commun.* 324:1199–1203. http://dx.doi.org/10.1016/j.bbrc.2004.09.176

da Silva Lopes, K., A. Pietas, M.H. Radke, and M. Gotthardt. 2011. Titin visualization in real time reveals an unexpected level of mobility within and between sarcomeres. *J. Cell Biol.* 193:785–798. http://dx.doi.org/10.1083/jcb.201010099

Dohke, T., A. Wada, T. Isono, M. Fujii, T. Yamamoto, T. Tsutamoto, and M. Horie. 2006. Proteomic analysis reveals significant alternations of cardiac small heat shock protein expression in congestive heart failure. *J. Card. Fail.* 12:77–84. http://dx.doi.org/10.1016/j.cardfail.2005.07.006

Donlin, L.T., C. Andresen, S. Just, E. Rudensky, C.T. Pappas, M. Kruger, E.Y. Jacobs, A. Unger, A. Zieseniss, M.W. Dobenecker, et al. 2012. Smyd2 controls cytoplasmic lysine methylation of Hsp90 and myofilament organization. *Genes Dev.* 26:114–119. http://dx.doi.org/10.1101/gad.177758.111

Doran, P., J. Gannon, K. O'Connell, and K. Ohlendieck. 2007. Aging skeletal muscle shows a drastic increase in the small heat shock proteins alphaB-crystallin/HspB5 and cvHsp/HspB7. *Eur. J. Cell Biol.* 86:629–640. http://dx.doi.org/10.1016/j.ejcb.2007.07.003

Ehrnsperger, M., H. Lilie, M. Gaestel, and J. Buchner. 1999. The dynamics of Hsp25 quaternary structure. Structure and function of different oligomeric species. *J. Biol. Chem.* 274:14867–14874. http://dx.doi.org/10.1074/jbc.274.21.14867

Fischer, D., J. Matten, J. Reimann, C. Bönnemann, and R. Schröder. 2002. Expression, localization and functional divergence of alphaB-crystallin and heat shock protein 27 in core myopathies and neurogenic atrophy. *Acta Neuropathol.* 104:297–304.

Fu, L., and J.J. Liang. 2003. Enhanced stability of alpha B-crystallin in the presence of small heat shock protein Hsp27. *Biochem. Biophys. Res. Commun.* 302:710–714. http://dx.doi.org/10.1016/S0006-291X(03)00257-2

Golenhofen, N., P. Htun, W. Ness, R. Koob, W. Schaper, and D. Drenckhahn. 1999. Binding of the stress protein alpha B-crystallin to cardiac myofibrils correlates with the degree of myocardial damage during ischemia/reperfusion in vivo. *J. Mol. Cell. Cardiol.* 31:569–580. http://dx.doi.org/10.1006/jmcc.1998.0892

Golenhofen, N., A. Arbeiter, R. Koob, and D. Drenckhahn. 2002. Ischemia-induced association of the stress protein alpha B-crystallin with I-band portion of cardiac titin. *J. Mol. Cell. Cardiol.* 34:309–319. http://dx.doi.org/10.1006/jmcc.2001.1513

Golenhofen, N., M.D. Perng, R.A. Quinlan, and D. Drenckhahn. 2004. Comparison of the small heat shock proteins alphaB-crystallin, MKBP, HSP25, HSP20, and cvHSP in heart and skeletal muscle. *Histochem. Cell Biol.* 122:415–425. http://dx.doi.org/10.1007/s00418-004-0711-z

Golenhofen, N., A. Redel, E.F. Wawrousek, and D. Drenckhahn. 2006. Ischemia-induced increase of stiffness of alphaB-crystallin/HSPB2-deficient myocardium. *Pflugers Arch.* 451:518–525. http://dx.doi.org/10.1007/s00424-005-1488-1

Hamdani, N., J. Krysiak, M.M. Kreusser, S. Neef, C.G. Dos Remedios, L.S. Maier, M. Krüger, J. Backs, and W.A. Linke. 2013. Crucial role for Ca2(+)/calmodulin-dependent protein kinase-II in regulating diastolic stress of normal and failing hearts via titin phosphorylation. *Circ. Res.* 112:664–674. http://dx.doi.org/10.1161/CIRCRESAHA.111.300105

Hegyi, H., and P. Tompa. 2008. Intrinsically disordered proteins display no preference for chaperone binding in vivo. *PLOS Comput. Biol.* 4:e1000017. http://dx.doi.org/10.1371/journal.pcbi.1000017

Houmeida, A., A. Baron, J. Keen, G.N. Khan, P.J. Knight, W.F. Stafford III, K. Thirumurugan, B. Thompson, L. Tskhovrebova, and J. Trinick. 2008. Evidence for the oligomeric state of 'elastic' titin in muscle sarcomeres. *J. Mol. Biol.* 384:299–312. http://dx.doi.org/10.1016/j.jmb.2008.09.030

Inaguma, Y., K. Hasegawa, S. Goto, H. Ito, and K. Kato. 1995. Induction of the synthesis of hsp27 and alpha B crystallin in tissues of heat-stressed rats and its suppression by ethanol or an alpha 1-adrenergic antagonist. *J. Biochem.* 117:1238–1243.

Khong, T.K., D.J. McIntyre, G.A. Sagnella, N.D. Markandu, M.A. Miller, E.H. Baker, J.R. Griffiths, and G.A. MacGregor. 2001. In-vivo intracellular pH at rest and during exercise in patients with essential hypertension. *J. Hypertens.* 19:1595–1600. http://dx.doi.org/10.1097/00004872-200109000-00011

Kienitz, M.C., K. Bender, R. Dermietzel, L. Pott, and G. Zoidl. 2011. Pannexin 1 constitutes the large conductance cation channel of cardiac myocytes. *J. Biol. Chem.* 286:290–298. http://dx.doi.org/10.1074/jbc.M110.163477

Klemenz, R., A.C. Andres, E. Fröhli, R. Schäfer, and A. Aoyama. 1993. Expression of the murine small heat shock proteins hsp 25 and alpha B crystallin in the absence of stress. *J. Cell Biol.* 120:639–645. http://dx.doi.org/10.1083/jcb.120.3.639

Kley, R.A., P. Serdaroglu-Oflazer, Y. Leber, Z. Odgerel, P.F. van der Ven, M. Olivé, I. Ferrer, A. Onipe, M. Mihaylov, J.M. Bilbao, et al. 2012. Pathophysiology

of protein aggregation and extended phenotyping in filaminopathy. *Brain*. 135:2642–2660. http://dx.doi.org/10.1093/brain/aws200

Knowlton, A.A., S. Kapadia, G. Torre-Amione, J.B. Durand, R. Bies, J. Young, and D.L. Mann. 1998. Differential expression of heat shock proteins in normal and failing human hearts. *J. Mol. Cell. Cardiol.* 30:811–818. http://dx.doi.org/10.1006/jmcc.1998.0646

Krüger, M., C. Sachse, W.H. Zimmermann, T. Eschenhagen, S. Klede, and W.A. Linke. 2008. Thyroid hormone regulates developmental titin isoform transitions via the phosphatidylinositol-3-kinase/AKT pathway. *Circ. Res.* 102:439–447. http://dx.doi.org/10.1161/CIRCRESAHA.107.162719

Lange, S., D. Auerbach, P. McLoughlin, E. Perriard, B.W. Schäfer, J.C. Perriard, and E. Ehler. 2002. Subcellular targeting of metabolic enzymes to titin in heart muscle may be mediated by DRAL/FHL-2. *J. Cell Sci.* 115:4925–4936. http://dx.doi.org/10.1242/jcs.00181

Larkins, N.T., R.M. Murphy, and G.D. Lamb. 2012. Absolute amounts and diffusibility of HSP72, HSP25, and αB-crystallin in fast- and slow-twitch skeletal muscle fibers of rat. *Am. J. Physiol. Cell Physiol.* 302:C228–C239. http://dx.doi.org/10.1152/ajpcell.00266.2011

Leake, M.C., D. Wilson, M. Gautel, and R.M. Simmons. 2004. The elasticity of single titin molecules using a two-bead optical tweezers assay. *Biophys. J.* 87:1112–1135. http://dx.doi.org/10.1529/biophysj.103.033571

Leake, M.C., A. Grützner, M. Krüger, and W.A. Linke. 2006. Mechanical properties of cardiac titin's N2B-region by single-molecule atomic force spectroscopy. *J. Struct. Biol.* 155:263–272. http://dx.doi.org/10.1016/j.jsb.2006.02.017

Li, H., W.A. Linke, A.F. Oberhauser, M. Carrion-Vazquez, J.G. Kerkvliet, H. Lu, P.E. Marszalek, and J.M. Fernandez. 2002. Reverse engineering of the giant muscle protein titin. *Nature*. 418:998–1002. http://dx.doi.org/10.1038/nature00938

Li, W., R. Rong, S. Zhao, X. Zhu, K. Zhang, X. Xiong, X. Yu, Q. Cui, S. Li, L. Chen, et al. 2012. Proteomic analysis of metabolic, cytoskeletal and stress response proteins in human heart failure. *J. Cell. Mol. Med.* 16:59–71. http://dx.doi.org/10.1111/j.1582-4934.2011.01336.x

Linding, R., J. Schymkowitz, F. Rousseau, F. Diella, and L. Serrano. 2004. A comparative study of the relationship between protein structure and beta-aggregation in globular and intrinsically disordered proteins. *J. Mol. Biol.* 342:345–353. http://dx.doi.org/10.1016/j.jmb.2004.06.088

Linke, W.A., and A. Grützner. 2008. Pulling single molecules of titin by AFM—recent advances and physiological implications. *Pflugers Arch.* 456:101–115. http://dx.doi.org/10.1007/s00424-007-0389-x

Linke, W.A., and M. Krüger. 2010. The giant protein titin as an integrator of myocyte signaling pathways. *Physiology (Bethesda)*. 25:186–198. http://dx.doi.org/10.1152/physiol.00005.2010

Linke, W.A., M. Ivemeyer, P. Mundel, M.R. Stockmeier, and B. Kolmerer. 1998. Nature of PEVK-titin elasticity in skeletal muscle. *Proc. Natl. Acad. Sci. USA*. 95:8052–8057. http://dx.doi.org/10.1073/pnas.95.14.8052

Linke, W.A., D.E. Rudy, T. Centner, M. Gautel, C. Witt, S. Labeit, and C.C. Gregorio. 1999. I-band titin in cardiac muscle is a three-element molecular spring and is critical for maintaining thin filament structure. *J. Cell Biol.* 146:631–644. http://dx.doi.org/10.1083/jcb.146.3.631

Liu, Y., and J.M. Steinacker. 2001. Changes in skeletal muscle heat shock proteins: pathological significance. *Front. Biosci.* 6:D12–D25. http://dx.doi.org/10.2741/Liu

Lu, X.Y., L. Chen, X.L. Cai, and H.T. Yang. 2008. Overexpression of heat shock protein 27 protects against ischaemia/reperfusion-induced cardiac dysfunction via stabilization of troponin I and T. *Cardiovasc. Res.* 79:500–508. http://dx.doi.org/10.1093/cvr/cvn091

Lutsch, G., R. Vetter, U. Offhauss, M. Wieske, H.J. Gröne, R. Klemenz, I. Schimke, J. Stahl, and R. Benndorf. 1997. Abundance and location of the small heat shock proteins HSP25 and alphaB-crystallin in rat and human heart. *Circulation*. 96:3466–3476. http://dx.doi.org/10.1161/01.CIR.96.10.3466

Marchetti, S., F. Sbrana, R. Raccis, L. Lanzi, C.M. Gambi, M. Vassalli, B. Tiribilli, A. Pacini, and A. Toscano. 2008. Dynamic light scattering and atomic force microscopy imaging on fragments of beta-connectin from human cardiac muscle. *Phys. Rev. E Stat. Nonlin. Soft Matter Phys.* 77:021910. http://dx.doi.org/10.1103/PhysRevE.77.021910

Markov, D.I., A.V. Pivovarova, I.S. Chernik, N.B. Gusev, and D.I. Levitsky. 2008. Small heat shock protein Hsp27 protects myosin S1 from heat-induced aggregation, but not from thermal denaturation and ATPase inactivation. *FEBS Lett.* 582:1407–1412. http://dx.doi.org/10.1016/j.febslet.2008.03.035

Martin, J., T. Langer, R. Boteva, A. Schramel, A.L. Horwich, and F.U. Hartl. 1991. Chaperonin-mediated protein folding at the surface of groEL through a 'molten globule'-like intermediate. *Nature*. 352:36–42. http://dx.doi.org/10.1038/352036a0

Martin, J.L., R. Mestril, R. Hilal-Dandan, L.L. Brunton, and W.H. Dillmann. 1997. Small heat shock proteins and protection against ischemic injury in cardiac myocytes. *Circulation*. 96:4343–4348. http://dx.doi.org/10.1161/01.CIR.96.12.4343

Melkani, G.C., A. Cammarato, and S.I. Bernstein. 2006. alphaB-crystallin maintains skeletal muscle myosin enzymatic activity and prevents its aggregation under heat-shock stress. *J. Mol. Biol.* 358:635–645. http://dx.doi.org/10.1016/j.jmb.2006.02.043

Minajeva, A., M. Kulke, J.M. Fernandez, and W.A. Linke. 2001. Unfolding of titin domains explains the viscoelastic behavior of skeletal myofibrils. *Biophys. J.* 80:1442–1451. http://dx.doi.org/10.1016/S0006-3495(01)76116-4

Miyake, S., Y. Ishii, T. Watari, Z. Huang, and T. Tsuchiya. 2003. The influences of L(+)-lactate and pH on contractile performance in rabbit glycerinated skeletal muscle. *Jpn. J. Physiol.* 53:401–409. http://dx.doi.org/10.2170/jjphysiol.53.401

Monsellier, E., and F. Chiti. 2007. Prevention of amyloid-like aggregation as a driving force of protein evolution. *EMBO Rep.* 8:737–742. http://dx.doi.org/10.1038/sj.embor.7401034

Morton, J.P., A.C. Kayani, A. McArdle, and B. Drust. 2009. The exercise-induced stress response of skeletal muscle, with specific emphasis on humans. *Sports Med.* 39:643–662. http://dx.doi.org/10.2165/00007256-200939080-00003

Mymrikov, E.V., A.S. Seit-Nebi, and N.B. Gusev. 2011. Large potentials of small heat shock proteins. *Physiol. Rev.* 91:1123–1159. http://dx.doi.org/10.1152/physrev.00023.2010

Neagoe, C., M. Kulke, F. del Monte, J.K. Gwathmey, P.P. de Tombe, R.J. Hajjar, and W.A. Linke. 2002. Titin isoform switch in ischemic human heart disease. *Circulation*. 106:1333–1341. http://dx.doi.org/10.1161/01.CIR.0000029803.93022.93

Olsson, M.C., M. Krüger, L.H. Meyer, L. Ahnlund, L. Gransberg, W.A. Linke, and L. Larsson. 2006. Fibre type-specific increase in passive muscle tension in spinal cord-injured subjects with spasticity. *J. Physiol.* 577:339–352. http://dx.doi.org/10.1113/jphysiol.2006.116749

Opitz, C.A., M.C. Leake, I. Makarenko, V. Benes, and W.A. Linke. 2004. Developmentally regulated switching of titin size alters myofibrillar stiffness in the perinatal heart. *Circ. Res.* 94:967–975. http://dx.doi.org/10.1161/01.RES.0000124301.48193.E1

Orchard, C.H., and J.C. Kentish. 1990. Effects of changes of pH on the contractile function of cardiac muscle. *Am. J. Physiol.* 258:C967–C981.

Paulsen, G., F. Lauritzen, M.L. Bayer, J.M. Kalhovde, I. Ugelstad, S.G. Owe, J. Hallén, L.H. Bergersen, and T. Raastad. 2009. Subcellular movement and expression of HSP27, alphaB-crystallin, and HSP70 after two bouts of eccentric exercise in humans. *J. Appl. Physiol.* 107:570–582. http://dx.doi.org/10.1152/japplphysiol.00209.2009

Pinz, I., J. Robbins, N.S. Rajasekaran, I.J. Benjamin, and J.S. Ingwall. 2008. Unmasking different mechanical and energetic roles for the small heat shock proteins CryAB and HSPB2 using genetically modified mouse hearts. *FASEB J.* 22:84–92. http://dx.doi.org/10.1096/fj.07-8130com

Rief, M., M. Gautel, F. Oesterhelt, J.M. Fernandez, and H.E. Gaub. 1997. Reversible unfolding of individual titin immunoglobulin domains by AFM. *Science*. 276:1109–1112. http://dx.doi.org/10.1126/science.276.5315.1109

Sheikh, F., A. Raskin, P.H. Chu, S. Lange, A.A. Domenighetti, M. Zheng, X. Liang, T. Zhang, T. Yajima, Y. Gu, et al. 2008. An FHL1-containing complex within the cardiomyocyte sarcomere mediates hypertrophic biomechanical stress responses in mice. *J. Clin. Invest.* 118:3870–3880. (published erratum appears in *J. Clin. Invest.* 2012. 122:1584. http://dx.doi.org/10.1172/JCI34472

Singh, B.N., K.S. Rao, T. Ramakrishna, N. Rangaraj, and ChM. Rao. 2007. Association of alphaB-crystallin, a small heat shock protein, with actin: role in modulating actin filament dynamics in vivo. *J. Mol. Biol.* 366:756–767. http://dx.doi.org/10.1016/j.jmb.2006.12.012

Somkuti, J., Z. Mártonfalvi, M.S. Kellermayer, and L. Smeller. 2013. Different pressure-temperature behavior of the structured and unstructured regions of titin. *Biochim. Biophys. Acta*. 1834:112–118. http://dx.doi.org/10.1016/j.bbapap.2012.10.001

Sun, Y., and T.H. MacRae. 2005. Small heat shock proteins: molecular structure and chaperone function. *Cell. Mol. Life Sci.* 62:2460–2476. http://dx.doi.org/10.1007/s00018-005-5190-4

Tskhovrebova, L., and J. Trinick. 1997. Direct visualization of extensibility in isolated titin molecules. *J. Mol. Biol.* 265:100–106. http://dx.doi.org/10.1006/jmbi.1996.0717

Tucker, N.R., and E.A. Shelden. 2009. Hsp27 associates with the titin filament system in heat-shocked zebrafish cardiomyocytes. *Exp. Cell Res.* 315:3176–3186. http://dx.doi.org/10.1016/j.yexcr.2009.06.030

Ulbricht, A., F.J. Eppler, V.E. Tapia, P.F. van der Ven, N. Hampe, N. Hersch, P. Vakeel, D. Stadel, A. Haas, P. Saftig, et al. 2013. Cellular mechanotransduction relies on tension-induced and chaperone-assisted autophagy. *Curr. Biol.* 23:430–435. http://dx.doi.org/10.1016/j.cub.2013.01.064

van de Klundert, F.A., M.L. Gijsen, P.R. van den IJssel, L.H. Snoeckx, and W.W. de Jong. 1998. alpha B-crystallin and hsp25 in neonatal cardiac cells—differences in cellular localization under stress conditions. *Eur. J. Cell Biol.* 75:38–45. http://dx.doi.org/10.1016/S0171-9335(98)80044-7

Vaughan-Jones, R.D., K.W. Spitzer, and P. Swietach. 2009. Intracellular pH regulation in heart. *J. Mol. Cell. Cardiol.* 46:318–331. http://dx.doi.org/10.1016/j.yjmcc.2008.10.024

Verschuure, P., Y. Croes, P.R. van den IJssel, R.A. Quinlan, W.W. de Jong, and W.C. Boelens. 2002. Translocation of small heat shock proteins to the actin cytoskeleton upon proteasomal inhibition. *J. Mol. Cell. Cardiol.* 34:117–128. http://dx.doi.org/10.1006/jmcc.2001.1493

Vicart, P.A., A. Caron, P. Guicheney, Z. Li, M.C. Prévost, A. Faure, D. Chateau, F. Chapon, F. Tomé, J.M. Dupret, et al. 1998. A missense mutation in the alphaB-crystallin chaperone gene causes a desmin-related myopathy. *Nat. Genet.* 20:92–95. http://dx.doi.org/10.1038/1765

Wang, X., R. Klevitsky, W. Huang, J. Glasford, F. Li, and J. Robbins. 2003. AlphaB-crystallin modulates protein aggregation of abnormal desmin. *Circ. Res.* 93:998–1005. http://dx.doi.org/10.1161/01.RES.0000102401.77712.ED

Willis, M.S., and C. Patterson. 2010. Hold me tight: Role of the heat shock protein family of chaperones in cardiac disease. *Circulation*. 122:1740–1751. http://dx.doi.org/10.1161/CIRCULATIONAHA.110.942250

Witt, C.C., B. Gerull, M.J. Davies, T. Centner, W.A. Linke, and L. Thierfelder. 2001. Hypercontractile properties of cardiac muscle fibers in a knock-in mouse model of cardiac myosin-binding protein-C. *J. Biol. Chem.* 276:5353–5359. http://dx.doi.org/10.1074/jbc.M008691200

Wright, C.F., S.A. Teichmann, J. Clarke, and C.M. Dobson. 2005. The importance of sequence diversity in the aggregation and evolution of proteins. *Nature*. 438:878–881. http://dx.doi.org/10.1038/nature04195

Yoshida, K., T. Aki, K. Harada, K.M. Shama, Y. Kamoda, A. Suzuki, and S. Ohno. 1999. Translocation of HSP27 and MKBP in ischemic heart. *Cell Struct. Funct.* 24:181–185. http://dx.doi.org/10.1247/csf.24.181

Zhu, Y., J. Bogomolovas, S. Labeit, and H. Granzier. 2009. Single molecule force spectroscopy of the cardiac titin N2B element: effects of the molecular chaperone alphaB-crystallin with disease-causing mutations. *J. Biol. Chem.* 284:13914–13923. http://dx.doi.org/10.1074/jbc.M809743200